Simultaneous propagation of hydraulic fractures from multiple perforation clusters in layered tight reservoirs: Non-planar three-dimensional modelling

Lei Yang [a, b], Shan Wu [b], Ke Gao [b], Luming Shen [a, *]

[a] School of Civil Engineering, The University of Sydney, NSW, 2006, Australia
[b] Department of Earth and Space Sciences, Southern University of Science and Technology, Shenzhen, Guangdong, 518055, China

ARTICLE INFO

ABSTRACT

In this paper, a hydromechanical coupled finite-discrete element method, which considers the non-planar three-dimensional growth, pressure continuity along the horizontal well, dynamic flow rate distributions among clusters, perforation friction, and fracturing fluid leakage, is employed to simulate the simultaneous growth of hydraulic fractures from an array of five perforation clusters in tight reservoirs interbedded with alternating stiff and soft layers. The simulation results highlight that the stress shadow induced by the non-planar propagation of the outmost hydraulic fractures stops the planar growth of the interior and middle hydraulic fractures and causes uneven fracturing fluid distribution among perforation clusters. The results demonstrate that the generated fracture pattern in the stage becomes more symmetric overall with the decreasing modulus of the soft layers. As the soft layer's modulus decreases, the total fracture height decreases significantly, but the local fracture aperture distribution increases, which leads to the reduction of total fracture area and leak-off volume of fracturing fluid as well as the increase of total fracture volume. The total fracture area decreases with the increasing leak-off coefficient and perforation number, but the total leak-off volume and total fracture volume increase. The violation of the fluid pressure continuity by without considering the dynamic flow rate distributions overestimates the growth of the interior and middle hydraulic fractures and produces a smaller total fracture area. It is also found that the adjustment of pumping rate is more effective than using nonuniform cluster spacing in promoting the simultaneous hydraulic-fracture growth in layered tight reservoirs.

© 2022 Elsevier Ltd. All rights reserved.

1. Introduction

Fluid-driven fracturing is of great significance in various natural and engineering activities. The commonly observed fluid-driven fractures in nature are the magma transport (dyke) in the lithosphere driven by buoyancy [1] and the fluid-filled cracks in glacier beds [2]. The artificial fluid-driven fracturing, known as hydraulic fracturing, aims to fracture the rock formation and enhance its permeability by injecting a large volume of fluid into the formation under high pressure. The prediction of hydraulic fracture propagation behaviour has attracted huge interest, as this technique has been used in a broad range of applications, such as stimulation of unconventional low-permeability reservoirs, carbon-capture storage, enhanced geothermal system, and nuclear waste disposal [3–5].

With the improvement of horizontal drilling technique, multi-stage and multi-cluster hydraulic fracturing technique has recently become one of the most effective methods in fracturing tight reservoirs with such small and poorly connected pores that the hydrocarbons (e.g., shale/tight gas and shale oil) cannot flow through them easily [6]. In this technique, a horizontal well is usually fractured at stages, and each fracturing stage comprises an array of perforation clusters, expected to initiate and propagate simultaneously [7,8]. In practice, the spacing among perforation clusters can range from several meters to tens of meters, and the productivity can be enhanced with smaller cluster spacings and more proppants [5,9]. It is estimated that the multi-cluster fracturing technique will play a significant role in the uplift of the U.S.

natural gas production from 24.1 trillion ft^3 in 2012 to 37.5 trillion ft^3 in 2040 [10–12].

The production logs from more than 100 horizontal shale wells in multiple basins indicate that only two-thirds of the perforation clusters contribute to the shale gas production, while other perforation clusters show impeded growth and poor productivity [13]. It was also identified by Spain et al. [14] that the stimulation of tight reservoirs is inefficient, as 40%−60% of perforation clusters have little or no production. Therefore, an in-depth understanding of the simultaneous propagation of hydraulic fractures from multiple perforation clusters within a fracturing stage is beneficial to maximizing the productivity in stimulating tight reservoirs. Due to the difficulty and cumbersomeness in identifying the evolution process and interaction behaviour of hydraulic fractures in the field, three-dimensional (3D) numerical simulators aimed at practical hydraulic fracturing treatment design are often developed as an advanced tool to investigate the simultaneous growth of multiple hydraulic fractures at field-scale. Overall, the reported simulators for practical design can be divided into two categories based on their simulated fracture geometries, including planar [9,15,16] and non-planar [17−21] 3D fracturing models. Note that the non-planar model can also simulate the planar growth of hydraulic fracture. The numerical methods used in these fracturing models include finite element method coupled with surface discontinuities [17], implicit level-set method [9], displacement discontinuity method [18,19], finite element-displacement discontinuity method [20], finite volume-displacement discontinuity method [15,16], and finite element-finite volume-boundary element method [21].

Indeed, the numerical results obtained from these fracturing models shed light on our understanding of the simultaneous propagation behaviour of multiple hydraulic fractures. In particular, the effects of cluster spacing, in-situ stress, perforation design, propagation regime, and leak-off have been discussed extensively. It is worth mentioning that simplifications are often made in these fracturing models mentioned above. For example, the fracturing model developed by Salimzadeh et al. [17] assumed the same flow rate but different injection pressures among perforation clusters, which violates the pressure continuity and dynamic flow rate distribution in the horizontal well. The planar [9,15] or constant-height [18] models limit the deflection and curving growth as well as the fracture height variation of hydraulic fractures. The non-planar fracturing models [18,19] based on 3D displacement discontinuity method restrict the fracture to be vertical, limiting their capability in describing complex fracture geometries. Kumar and Ghassemi [20] presumed the negligible fracturing fluid leak-off in their model due to the ultralow permeability of tight reservoirs, which is contradictory with the large leak-off of fracturing fluid observed in the field [22]. Also, in the reported fracturing models [9,17,21], the perforation friction is neglected, and a single fracture is assumed per cluster.

Another simplification often employed in the reported 3D multi-cluster fracturing models is treating the tight reservoirs as a homogeneous media. Log profiles and cores show that many tight reservoirs are interbedded and stratified with layers performing different material properties (e.g., Young's modulus), and the layer thickness varies from centimetres to meters, e.g., the Eagle Ford shale reservoir interbedded with alternating stiff carbonate-rich layers and soft clay-rich layers [23−25]. The modulus contrast between alternating stiff and soft layers in tight reservoirs are arduous to implement in 3D multi-cluster fracturing models, especially those based on boundary element method and displacement discontinuity method. In consequence, the layered modulus effect of tight reservoir is often neglected in most of 3D multi-cluster fracturing simulators. There are several analytical solutions that calculate the effective modulus of layered reservoir

and can be used in numerical modelling for convenience [26,27]. Under this condition, the layered reservoir is simplified as a homogenous reservoir whose elastic modulus equals the effective modulus of the combined layers. However, these analytical solutions are proposed for the planar growth of hydraulic fracture, which is not suitable for describing the non-planar 3D fractures commonly observed in multi-cluster fracturing.

To sum up, the multi-cluster fracturing in tight reservoirs involves multiple physical processes, including basic (e.g., the rock deformation, fracture initiation and propagation, fracture fluid flow, and porous flow) and secondary (e.g., fluid flow in the horizontal well, perforation friction, leak-off, poroelastic effect, and alternated layers of tight formations) physical processes [28]. Investigating the simultaneous growth behaviour of multiple hydraulic fractures requires a 3D multi-cluster fracturing simulator capable of modelling these physical processes together. Per the authors' knowledge, the relevant studies are very limited. Only several studies [29,30] simulated the non-planar 3D multi-fracturing process in three-layered formations that usually consisted of two barrier layers and one reservoir layer. Their interests were the containment effect of the pay zone layer on the propagation of multiple hydraulic fractures in the reservoir layer, and the reservoir layer was homogeneous without alternating layers. Therefore, in this study, a versatile numerical simulator Elfen TGR [31], which is based on the hydromechanical coupled finite-discrete element method (FDEM), is employed to investigate the simultaneous hydraulic-fracture propagation in tight reservoirs interbedded with alternating stiff and soft layers. The Elfen TGR can model the complex geometries (e.g., planar and non-planar) of simultaneously evolving hydraulic fractures and the associated multiple physical processes in 3D space. In particular, the effect of layer modulus ratio on the simultaneous propagation mechanism and behaviour is investigated, and the methods to promote the simultaneous growth are compared and discussed.

The remaining sections of the paper are organised as follows. Mathematical equations to describe the hydromechanical coupled FDEM of Elfen TGR are presented in Section 2. The 3D tight reservoir model interbedded with alternating stiff (high Young's modulus) and soft (low Young's modulus) layers is illustrated in Section 3. The layered tight reservoir is stimulated by an array of five perforation clusters closely spaced within one fracturing stage, and the modulus contrast between stiff and soft layers is varied to explore the layered modulus effect. Simulations results are summarised and discussed in Section 4. The discussion on promoting simultaneous growth is also presented. Finally, the conclusions drawn from this work are encapsulated in Section 5.

2. Finite-discrete element method for hydromechanical modelling

The Elfen TGR is developed by Rockfiled Inc. based on the FDEM, aiming at simulating the complex coupled geomechanical and hydraulic systems in tight reservoirs [31]. It has multifarious advantages: (i) simulating the propagation and interaction of non-planar hydraulic fractures in 3D; (ii) considering leak-off, perforation friction, proppant transport, fracture closure, flow back, heterogeneity, hydraulic-natural fracture interactions and stress shadow effect; (iii) allowing multi-well, multi-stage, and multi-cluster stimulations; and (iv) establishing elastic-plastic reservoir models coupled with fracture fluid flow and porous flow [28]. Moreover, Elfen TGR is an all-in-one simulator and allows the modelling of the entire cycle of stimulation-production-refracturing-production operations. Its capability in hydraulic fracturing treatment design has been demonstrated in several studies [32−34]. Here, only the stimulation operation in Elfen TGR is considered, and the

mathematical equations to describe the hydromechanical coupled FDEM is given in this section. More details relating to the numerical algorithms of Elfen TGR can be found in Profit et al. [32].

2.1. Geomechanical equations

The petroleum-bearing rock formations are a typical porous media, and its hydraulic fracturing process involves the coupling between the effective stress field in the rock formation, the pore fluid flow in the rock formation, and the fluid flow in the fracture region. The associated three sets of governing equations are the structure field, seepage field and network field, respectively.

The structure field relates to the equilibrium of mechanical stress and pore fluid pressure in the rock formation with external loads, and its governing equation is expressed as [35].

$$\mathbf{L^T}(\boldsymbol{\sigma}^e - \alpha \mathbf{m} p_s) + \rho_b \mathbf{g} = \mathbf{0}, \tag{1}$$

where $\mathbf{L}$ is the spatial differential operator; $\boldsymbol{\sigma}^e$ is the effective stress; α is the Biot coefficient; $\mathbf{m}$ is the identity tensor; p_s is the rock formation's pore fluid pressure; ρ_b is the wet bulk density of rock; and $\mathbf{g}$ is the vector of gravity.

The seepage field describes the porous flow in the rock formation, and its governing equation integrates mass conversation with Darcy's law and is given as [35].

$$\nabla \cdot \left[\frac{k}{\mu_l} (\nabla p_l - \rho_l \mathbf{g}) \right] = \left(\frac{\varphi}{K_l} + \frac{\alpha - \varphi}{K_s} \right) \frac{\partial p_l}{\partial t} + \alpha \frac{\partial \varepsilon_v}{\partial t}, \tag{2}$$

where k is the intrinsic permeability of the porous rock formation; μ_l is the viscosity of the pore fluid; p_l is the pore fluid pressure; ρ_l is the pore fluid density; φ is the porosity of the rock formation; K_l is the bulk modulus of the pore fluid; K_s is the bulk modulus of the solid grains; and ε_v is the volumetric strain of the rock formation.

Like the seepage field, the network field combines mass conversation along with Darcy's law to describe the fluid flow in the fracture region. In the network field, it is assumed that the fracturing fluid is incompressible, laminar with a low Reynolds number and locally similar to the parallel-plate flow. The governing equation of network field is written as [32].

$$\nabla \cdot \left[\frac{k^{fr}}{\mu_n} \left(\nabla p_n - \rho_{fn} \mathbf{g} \right) \right] = S^{fr} \frac{\partial p_n}{\partial t} + \alpha (\Delta \dot{e}_\varepsilon), \tag{3}$$

where k^{fr} is the intrinsic permeability of the fractured region; μ_n is the fracturing fluid's viscosity; p_n is the pressure of the fracturing fluid; ρ_{fn} is the fracturing fluid's density; S^{fr} is the storage coefficient of the rock formation; and $\dot{e}_\varepsilon$ is the strain rate of fracture aperture. Based on the theory of parallel plate flow, both k^{fr} and S^{fr} relate to the fracture aperture. The intrinsic permeability of fractured region is defined as [36].

$$k^{fr} = \frac{e^2}{12}, \tag{4}$$

where e is the fracture aperture. The storage coefficient is written as [35].

$$S^{fr} = \left(\frac{1}{e} \right) \left(\frac{1}{K_n^{fr}} + \frac{e}{K_f^{fr}} \right), \tag{5}$$

where K_n^{fr} is the normal stiffness of the fracture; and K_f^{fr} is the fracturing fluid's bulk modulus.

2.2. Fracturing fluid leak-off

Field observations in the petroleum industry show that 50%–80% of injected fluid can be lost when stimulating a tight reservoir [37]. Hence, a reliable hydromechanical model needs to take this behaviour into account to obtain the correct stimulated fracture area and volume. In this study, the leak-off effect is considered by employing the 1D Carter leak-off model which assumes that the filter cake forms on the exposed fracture surface over time [38]. At the start, the tight reservoir's flow characteristics, such as the intrinsic permeability, determine the leak-off degree of fracturing fluid. Once the filter cake forms, it controls the fluid leak-off. The model presumes an initial volume loss V_{sp} per unit area over a spurt time t_{sp} succeeded by a constant leak-off coefficient C. The leak-off model is formulated as [32].

$$t - t_{\exp} < t_{sp}; \ q_l = \frac{V_{sp}}{t_{sp}},$$

$$t - t_{\exp} \geq t_{sp}; \ q_l = \frac{C}{\sqrt{t - t_{\exp}}}, \tag{6}$$

where t is the current time; $t_{\exp}$ is the time when the fracture surface is exposed to leak-off; q_l is the 1D leak-off velocity of fracture fluid in the normal direction. The spurt volume is determined based on the result of fluid loss experiment [39].

2.3. Fluid flow in the horizontal well

In the multi-cluster fracturing treatment, the fracturing fluid flows along the horizontal well and distributes into each perforation clusters dynamically. The storage effect of the horizontal well is ignored here, and thus, for a specified total volumetric flow rate Q, the flow rate into each perforation cluster Q_i meets [18].

$$Q = \sum_{i=1}^{n} Q_i, \tag{7}$$

where n is the identification number of perforation cluster. Since the perforation clusters within a fracturing stage are often closely spaced, the horizontal well's friction among them can be neglected [7,40,41]. The pressure continuity along the horizontal well is then expressed as [18].

$$P_{hw} = P_{pf,i} + P_{in,i}, \tag{8}$$

where P_{hw} is the fluid pressure of the horizontal well; $P_{in,i}$ is the inlet pressure of the ith perforation cluster; and $P_{pf,i}$ is the perforation pressure drop in the ith perforation cluster, which is determined as [42].

$$P_{pf,i} = \frac{8\rho_{fn}}{\pi^2 C_D^2 d_p^4} \left(\frac{Q_i}{N_p} \right)^2, \tag{9}$$

where C_D is the discharge coefficient; d_p is the diameter of perforation; and N_p is the number of perforations.

2.4. Fracture criteria

The rock formation's stresses are controlled by the elasticity, Mohr-Coulomb plasticity, and Rankine tensile failure. Here, the Mohr-Coulomb and Rankine constitutive models are combined into a single yield surface envelope to describe the failure in tension and the following fracture, as shown in Fig. 1(a) [32]. In Fig. 1(a), σ_1, σ_2
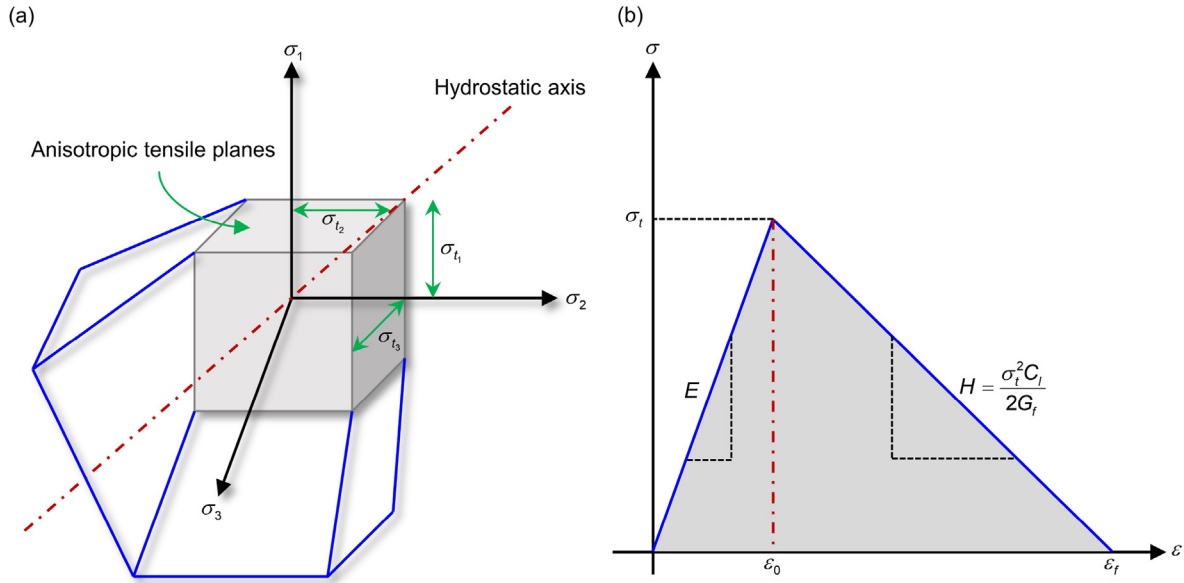
Fig. 1. (a) A single yield surface combining Mohr-Coulomb model with Rankine tensile corner in the principal stress space, and (b) a typical stress-strain response of a quasi-brittle material under uniaxial tension.

and σ_3 are the three principal stresses, and σ_{t1}, σ_{t2} and σ_{t3} are the corresponding tensile strengths. In present study, the material property in each layer of the layered tight reservoirs is homogeneous for simplicity.

The Rankine tensile model plays a key role in the hydraulic fracturing, because the positive maximum principal stress at the fracture tip allows for the continued fracture propagation. A typical continuum stress-strain relationship for a quasi-brittle rock material under tension is plotted in Fig. 1(b). In the plot, ε_0 and ε_f are the strains at uniaxial yield and failure points, respectively. In the pre-yield stage, the rock behaves elastically, and its deformation behaviour is governed by the Young's modulus E and Poisson's ratio v. Once the rock reaches its tensile strength at the yield point, it starts to soften and finally fail when its fracture energy has been released. The post-yield regime of rock only depends on its tensile strength σ_t and fracture energy G_f, and its softening slope H is calculated as [32].

$$H = \frac{\sigma_t^2 C_l}{2G_f},\tag{10}$$

where C_l is the characteristic length of an element, and its incorporation is to ensure the objective energy dissipation in arbitrary meshes. In the FDEM, the explicit fracture can be formed in the formation by rupturing the nodes once the rock material fails completely.

2.5. Numerical discretion and coupling strategy for geomechanical equations

The primary target application of this study is the hydraulic stimulation of tight gas from layered reservoirs. The effective resistance of the high compressible dry gas in the formation pores (e.g., methane) is insignificant compared with the effective stress generated in the tight formation. In consequence, the seepage field relating to the porous flow in the rock formation is considered uncoupled with the structure field and is only included to satisfy the completeness of the equilibrium equation here. The governing equations of structure field and network field can be semi-

discretised by using finite element method. Here, it is assumed the shape functions for structure, seepage and network fields can be independent.

$$\mathbf{B}_u = \mathbf{L}_u \mathbf{N}_u, \quad \mathbf{B}_s = \mathbf{L}_s \mathbf{N}_s, \quad \mathbf{B}_n = \mathbf{L}_n \mathbf{N}_n,\tag{11}$$

where $\mathbf{B}_u$, $\mathbf{B}_s$, and $\mathbf{B}_n$ are the shape function spatial gradient matrices for structure, seepage and network fields, respectively; $\mathbf{L}_u$, $\mathbf{L}_s$, and $\mathbf{L}_n$ are the gradient operators for the structure, seepage and network fields, respectively; $\mathbf{N}_u$, $\mathbf{N}_s$, and $\mathbf{N}_n$ are the corresponding matrices of shape functions of structure, seepage, and network fields, respectively.

The governing equation of structure field is discretised with the finite element and given as

$$\int_{\Omega_u} \mathbf{B}_u^{\mathrm{T}} \boldsymbol{\sigma}^e \partial\Omega_u - \int_{\Omega_s} \mathbf{B}_u^{\mathrm{T}} \alpha \mathbf{m} \mathbf{N}_s \partial\Omega_s p_s = \mathbf{f}_u,\tag{12}$$

where Ω_u is the structure domain; Ω_s is the seepage domain; and $\mathbf{f}_u$ is the mechanical load vector. The effective stress tensor $\boldsymbol{\sigma}^e$ in the structured field is calculated with the Mohr-Coulomb and Rankine tensile material models. The governing equation of finite element discretised network field is written as

$$\int_{\Omega_n} \mathbf{B}_u^{\mathrm{T}} \frac{k^{fr}}{\mu_n} \mathbf{B}_n p_n \partial\Omega_n - \int_{\Omega_s} \mathbf{N}_n^{\mathrm{T}} S^{fr} \mathbf{N}_n \partial\Omega_n \frac{\partial p_n}{\partial t} = \mathbf{f}_n,\tag{13}$$

where Ω_n is the domain of network field; and $\mathbf{f}_n$ is the fracture fluid load vector. One can couple the governing equations of structure and network fields in the form of matrix as

$$\begin{bmatrix} \mathbf{M} & 0 \\ 0 & 0 \end{bmatrix} \begin{bmatrix} \ddot{\mathbf{u}} \\ \ddot{p}_n \end{bmatrix} + \begin{bmatrix} 0 & 0 \\ \mathbf{Q}_n^{\mathrm{T}} & \mathbf{S}_n \end{bmatrix} \begin{bmatrix} \dot{\mathbf{u}} \\ \dot{p}_n \end{bmatrix} + \begin{bmatrix} \mathbf{K} & 0 \\ 0 & \mathbf{H}_n \end{bmatrix} \begin{bmatrix} \mathbf{u} \\ p_n \end{bmatrix} = \begin{bmatrix} \mathbf{f}_u \\ \mathbf{f}_n \end{bmatrix}\tag{14}$$

where the details of the matrix and vector can be referred to Profit et al. [32].

A staggered coupling scheme is employed in the

hydromechanical model, in which the structured field's governing equation is solved explicitly, while the network field's governing equation is solved implicitly. The fracture aperture's motion is calculated in the structure field and then transferred to the network field to update the permeability of the propagating fracture. Similarly, the fracture fluid pressure is calculated in the network field and then transferred into the adjacent structure field region. In the finite-discrete element method, the conventional finite element method is used to solve the problems in the continuum media, while the discrete element method works when the explicit fracture is formed by separating the connected nodes.

2.6. Validation of the hydromechanical model

The developed hydromechanical model is validated against an asymptotic solution proposed by Savitski and Detounary [43]. The solution assumes that a penny-shaped hydraulic fracture propagates in impermeable rock, and the fracturing fluid is incompressible without leak-off and fluid lag at the fracture tip. In the solution, a dimensional viscosity is defined to identify the propagation regime and is expressed as

$$M_\mu = \mu' \left(\frac{Q^3 E'^{13}}{K'^{13} t^2} \right)^{1/5},$$ (15)

where M_μ is the dimensional viscosity; $\mu' = 12\mu_n$; $E' = E/(1 - \nu^2)$; $K' = 4\sqrt{2/\pi}K_{IC}$; K_{IC} is the fracture toughness; t is the injection time. The penny-shape hydraulic fracture propagates in the viscosity-dominated regime when $M_\mu \gg 1$ and in toughness-dominated regime when $M_\mu \ll 1$. The energy dissipated in the fluid flow within fracture is dominant compared to that in the fracture surface creation for the viscosity-dominated regime, and vice versus for the toughness-dominated regime. In this validation, a group of parameters is designed, i.e., $E = 32$ GPa, $\nu = 0.2$, $\mu_n = 10$ Pa·s$K_{IC} = 1.26$ MPa·m$^{0.5}$, $Q = 0.02$ m^3/s, and $t = 150$ s, given that $M_\mu = 2.38 \times 10^{10} \gg 1$. The radius and injection pressure evolutions of a viscosity-dominated penny-shaped hydraulic fracture are formulated as [43].

$$R(t) = 0.6955 \left(\frac{E'Q_0^3 t^4}{\mu'} \right)^{1/9},$$ (16)

$$P(t) = 0.24289 \left(\frac{\mu' E'^2}{t} \right)^{1/3},$$ (17)

where $R(t)$ and $P(t)$ are the hydraulic fracture radius and fluid injection pressure at time t, respectively. In the numerical simulation, a 3D model with a dimension of 100 m × 100 m × 60 m (length × width × height) is established. The initial penny-shaped hydraulic fracture has a radius of 2.5 m and is meshed by triangle elements with a size of 0.25 m, and the impermeable rock domain is meshed by tetrahedral elements with a size of 0.5 m. The perforation friction and fracturing fluid leakage are not considered in the numerical simulation. Fig. 2(a) and Fig. 2(b) show the penny-shaped hydraulic fracture's radius evolution and the injection pressure evolution of the fracturing fluid obtained from the asymptotic solution and numerical simulation. It can be seen from the penny-shaped hydraulic fracture growth predicted by the present model is in good agreement with the asymptotic solution.

3. Numerical model setup and schemes.

Fig. 3 illustrates the numerical model of a layered tight reservoir stimulated by multiple perforation clusters placed within a given fracturing stage. As shown in the Fig. 3(a), the layered tight reservoir model has a dimension of 60 m × 60 m × 20 m (length × width × height) in the X-, Y-, and Z-directions, respectively. Such a dimension ensures that the model boundaries have an insignificant effect on our numerical cases. Fig. 3(b) plots that the layered tight reservoir is composed of two types of material layers alternated in the Z-direction. These two types of layers are referred as stiff and soft layers, since they have the same material properties and layer height except for the Young's modulus. Such an approach is often used in reported studies to evaluate the layered modulus effect [26,44,45]. Three stiff layers and two soft layers are interbedded in the layered tight reservoir, and each layer has a height of 4 m. This height is selected according to the log profiles and cores that show the layer height varies from centimetres to meters [23].
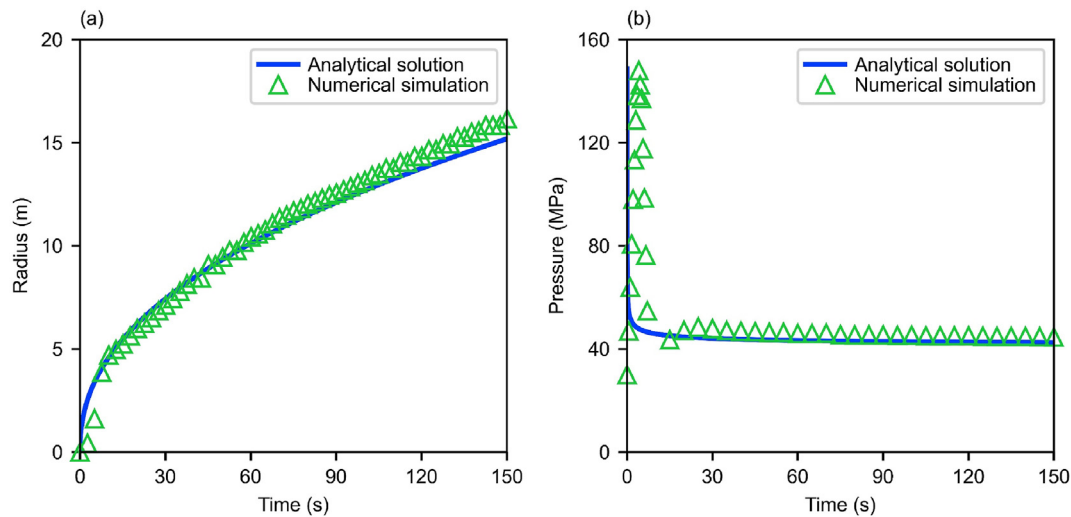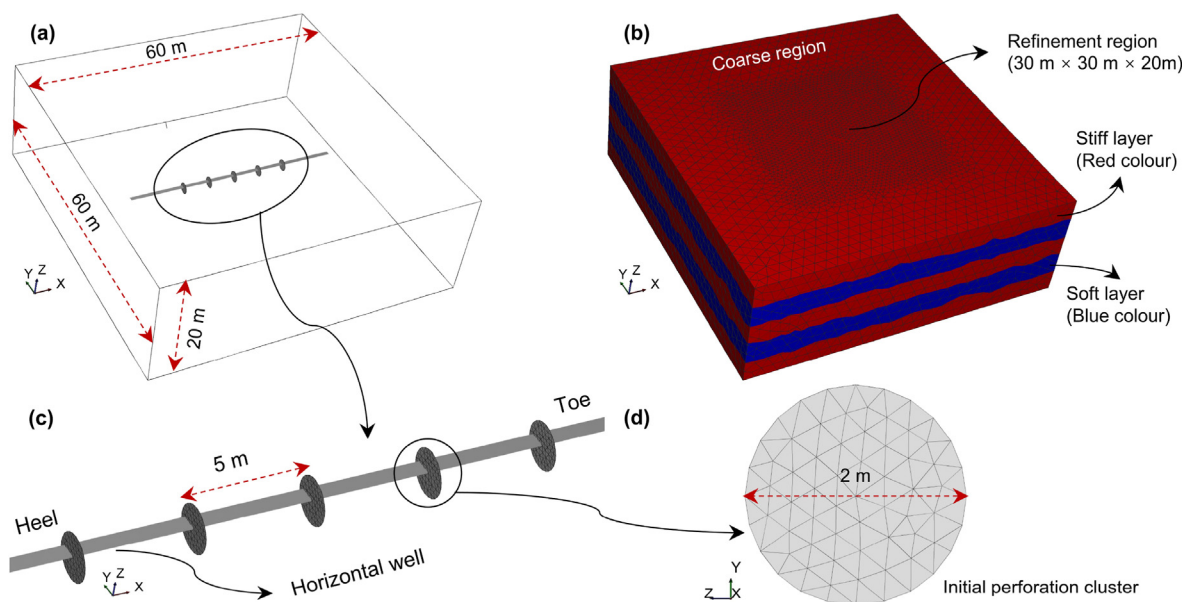

Fig. 2. Comparison of the (a) fracture radius and (b) injection pressure of a penny-shaped hydraulic fracture between numerical simulation and analytical solution.

Fig. 3. Finite-discrete element method model for the hydraulic stimulation of a layered tight reservoir: (a) geometrical dimension, (b) meshed reservoir with alternating stiff and soft layers, (c) five perforation clusters placed within a fracturing stage along the horizontal well, and (d) the meshed initial perforation cluster.

Tetrahedral and triangle elements are used to discretise the reservoir and initial perforation clusters in the Elfen TGR based on FDEM, respectively, to simulate the arbitrary propagation behaviour of hydraulic fractures. A total number of 224, 503 tetrahedral finite elements are used to discretise the layered reservoir after the mesh convergence study, making a trade-off between numerical accuracy and computational cost. The refinement region in which the perforation clusters grow has a smaller element size of 0.75 m, while the outside remote from the region of interest is meshed by coarse elements with a larger size of 2 m.

The horizontal well and initial perforation clusters are presented in Fig. 3(c). It is assumed that the fracturing stage has five perforation clusters propagating simultaneously, since in practice, one stage is typically aimed at initiating and propagating three to eight perforation clusters spaced about 10−30 m apart [15]. The spacing among perforation clusters is 5 m, and consequently, the perforation clusters are placed in a zone with its length close to the reservoir height, which is often the case in the practical multi-cluster and multi-stage fracturing [9]. The initial perforation clusters from the heel to the toe are referred to as 1st, 2nd, 3rd, 4th, and 5th perforation clusters in order. The outmost (1st and 5th), interior (2nd and 4th), and middle (3rd) perforation clusters are also used in the following sections. The initial perforation clusters are placed orthogonally to the horizontal well and intersect with the horizontal well at their centres. The fracturing fluid flows from the heel to the toe in the horizontal well and enters the perforation clusters at the intersection points between the perforation clusters and the horizontal well. The diameter of the perforation clusters in the reported numerical simulations is often between 2 m and 10 m [15,17,20]. Here, the initial perforation cluster has a diameter of 2 m and is meshed with an element size of 0.25 m, as shown in Fig. 3(d). The number of perforations, perforation diameter and perforation coefficient in each cluster are assumed equal to 4, 7.62 mm, and 0.78, respectively.

The material properties of the layered tight reservoir adopted from Profit et al. [32] are given in Table 1. In particular, the stiff layer's modulus is kept constant at 32 GPa, while the soft layer's modulus varies from 24 GPa to 4 GPa to investigate the layer modulus ratio effect on the simultaneous propagation of multiple

perforation clusters. *In-situ* stresses and pore pressure fields applied on the reservoir are listed in Table 2. The effective vertical stress (σ_V), effective minimum horizontal stress (σ_h), effective maximum horizontal stress (σ_H), and pore pressure are 20 MPa, 10 MPa, 12 MPa, and 30 MPa, respectively. The horizontal well is drilled parallel to the minimum horizontal stress. The total flow rate in the horizontal well is specified as 0.02 m³/s, while the flow rates into each perforation cluster are dynamically adjusted. The total flow rate in the horizontal well is equal to the sum of flow rates of all perforation clusters. The fracturing fluid with a viscosity of 0.001 Pa s is used to stimulate the layered reservoir, and a total volume of 5 m³ fracturing fluid is injected with a pumping duration of 250 s. The fracturing fluid properties and pumping schedule is summarised in Table 3.

The flow chart of a typical numerical simulation process is illustrated in Fig. 4. From this plot, one can see that the overall

Table 1
Material parameters of the layered tight reservoir.

Parameters	Symbol	Value	Unit
Young's modulus of stiff layer	E_{stiff}	32	GPa
Young's modulus of soft layer	E_{soft}	24, 16, 8, 4	GPa
Poisson's ratio	ν	0.2	−
Density	ρ_b	2700	kg/m³
Tensile strength	σ_t	1	MPa
Fracture energy	G_f	50	N/m
Grain bulk modulus	K_s	15.3	GPa
Permeability	k	4.9e-21	m²
Porosity	φ	0.05	−
Leak-off coefficient	C	1e-4	m/s$^{0.5}$

Table 2
In-situ stress and pore pressure.

Parameters	Symbol	Value	Unit
Vertical stress (Z-direction)	σ_V	20	MPa
Maximum horizontal stress (Y-direction)	σ_H	12	MPa
Minimum horizontal stress (X-direction)	σ_h	10	MPa
Pore pressure	p_s	30	MPa

Table 3
Fracturing fluid properties and pumping schedule.

Parameters	Symbol	Value	Unit
Fracturing fluid viscosity	μ_n	0.001	Pa·s
Bulk modulus of fracturing fluid	K_f^{fr}	2000	Mpa
Flow rate	Q	0.02	m³/s
Pumping volume	V	5	m³
Pumping duration	t	250	s

calculation process starts with the input of model dimensions, in-situ stress conditions, material properties of the layered tight reservoir and the fracturing fluid, and the pumping schedule. Then, the geometric model composed of the reservoir, horizontal well and initial perforation clusters is generated based on the pre-defined model dimensions. Next, tetrahedral elements are used to discretise the layered tight reservoir, and triangle elements are employed to discretise the horizontal well and initial perforation clusters. After applying the initial conditions on the 3D FDEM model, including in-situ stress, pore pressure and boundary conditions, the numerical calculation is triggered by injecting the fracturing fluid into the reservoir. During the model calculation, the staggered scheme is used for the coupling between the structure filed and network field. Once the fracturing fluid injection is terminated, the model outputs the hydromechanical solutions (e.g., stress field, fracturing fluid pressure), the quantitative and qualitative information of fracture pattern.
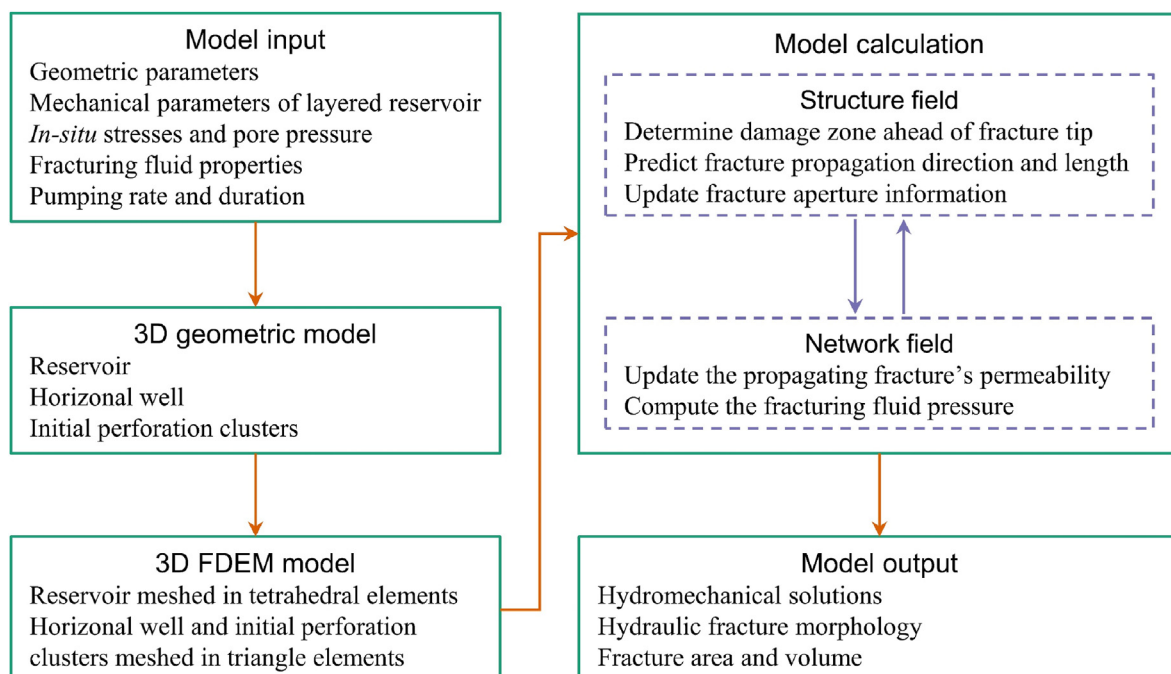
3. Simulation results and discussion

### 3.1. Simultaneous propagation mechanism of multiple hydraulic fractures in layered tight reservoirs

In the case of multi-cluster and multi-stage hydraulic fracturing, the multiple perforation clusters placed in the same fracturing stage are initiated and propagate simultaneously. During the fracturing fluid injection process, the pressurization of hydraulic fractures changes the stress state of the tight reservoir and then causes the tight reservoir deformation and fracture. In turn, the stress change in the tight reservoir influences the simultaneous propagation process of multiple hydraulic fractures [20]. The simultaneous propagation behaviours of hydraulic fractures from multiple perforation clusters in layered tight reservoirs with the soft layer's modulus between 24 GPa and 4 GPa overall are similar. Hence, only the case of the layered tight reservoir with the soft layer's modulus of 16 GPa is selected as the example to explore the underlying mechanism.

The hydraulic fractures' profile and maximum principal stress distribution in the layered tight reservoir at different injection times are illustrated in Fig. 5. At the beginning of fluid injection, the multiple hydraulic fractures propagate simultaneously and pla-narly, as shown in Fig. 5(a). The induced tensile stress at the fracture tip and the significant compressional regions adjacent to the opening fracture are known as stress shadow [46]. At this stage, the interference among the multiple hydraulic fractures is not strong, and the hydraulic fracture propagation is controlled by the in-situ stress difference which promotes the hydraulic fracture propa-gating planarly. As more fracturing fluid is injected and the hydraulic fractures grow larger, the magnified stress shadows coalesce with each other and overbalance the effect of the in-situ stress field. The strong stress shadow effect can lead to the non-planar propagation and stagnation of hydraulic fracture. For example, the outmost (1st and 5th) hydraulic fractures propagate non-planarly at t = 20 s, while the interior (2nd and 4th) and middle (3rd) hydraulic fractures keep growing planarly, as shown in Fig. 5(b). At t = 35 s, the middle hydraulic fracture has already been stagnated in both height and length directions, due to the formation of compressive stress umbrella at the fracture tip induced by the stress shadow coalesce of interior hydraulic fractures, as shown in Fig. 5(c). Once the stress shadows induced by the propagation of outmost hydraulic fractures coalesce with each other, compressive stress regions are also formed at the fracture tips of interior hydraulic fractures, resulting in their stagnation, as shown in Fig. 5(d). Note that the propagation of hydraulic fracture

Model input
Geometric parameters
Mechanical parameters of layered reservoir
In-situ stresses and pore pressure
Fracturing fluid properties
Pumping rate and duration

3D geometric model
Reservoir
Horizontal well
Initial perforation clusters

3D FDEM model
Reservoir meshed in tetrahedral elements
Horizonal well and initial perforation
clusters meshed in triangle elements

Model calculation

Structure field
Determine damage zone ahead of fracture tip
Predict fracture propagation direction and length
Update fracture aperture information

Network field
Update the propagating fracture's permeability
Compute the fracturing fluid pressure

Model output
Hydromechanical solutions
Hydraulic fracture morphology
Fracture area and volume

Fig. 4. Flow chart for modelling the non-planar 3D multi-fracture propagation in layered tight reservoirs.
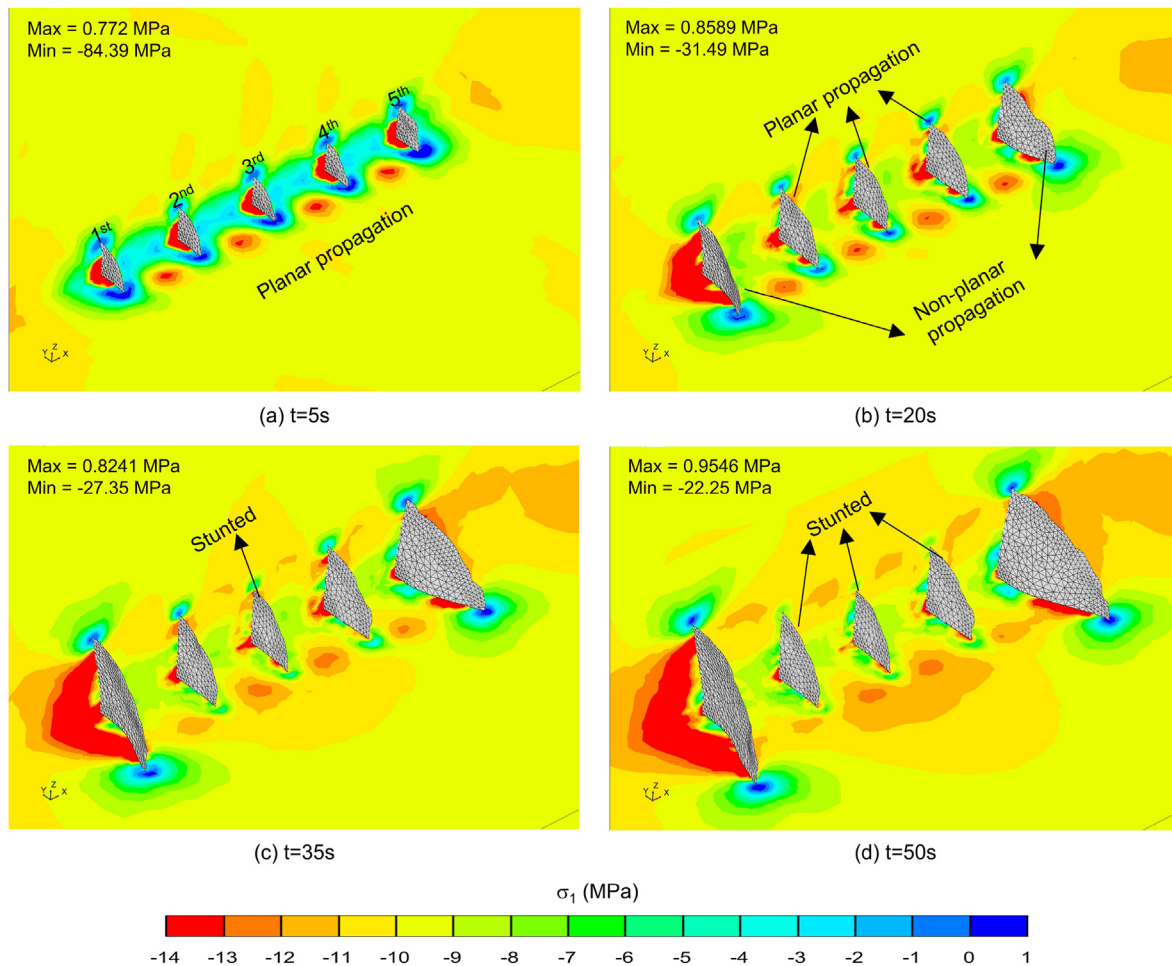
Fig. 5. Fracture profile and maximum principal stress evolutions of multiple hydraulic fractures in the layered tight reservoir. The figures are captured from the middle XY and XZ sections under the same region and angle, to illustrate the height growth in the positive Z-direction and the length growth in the negative Y-direction.

must ensure the tensile stress intensity generated by the fracturing fluid pressure exceeds the sum of the current maximum principal stress and the formation tensile strength. The compressive stress umbrellas formed at the fracture tips require a greater demand for further propagation of middle and interior hydraulic fractures. As a result, the hydraulic fracture propagation only occurs in the outmost hydraulic fractures whose tips are subjected to tensile stress or minimum compression stress with the least resistance.

The morphology and aperture of the 3D hydraulic fractures corresponding to the injection times in Fig. 5 are illustrated in Fig. 6. In Fig. 6, the grey part denotes the horizontal well and the fracturing fluid flows from the heel to the toe. A shown in the figure, the outmost hydraulic fractures propagate non-planarly and deflect significantly at their peripheries, while the middle and interior fractures do not produce any evident deflection. In addition, the openings of the middle and interior hydraulic fractures are gradually constrained and reduced to the minimum fracture aperture (e.g., 0.05 mm for the newly created hydraulic fractures) due to the significant compressional stress induced by the propagation of the outmost hydraulic fractures. Whether the hydraulic fracture propagates in planarly or non-planarly depends on the generated shear stress. The evolutions of the shear stresses at the middle XY and XZ sections are illustrated in Fig. 7. Since no *in-situ* shear stresses are applied in the layered tight reservoir, the shear stress is induced by the propagation of hydraulic fractures. It can be seen from Fig. 7 that at t = 5 s, the shear stresses on the left and right

sides of each hydraulic fracture are symmetric, i.e., similar magnitudes but opposite in sign. Consequently, all hydraulic fractures propagate planarly at the beginning of fracturing fluid injection. As the hydraulic fractures grow in height and length directions, the generated shear stresses interact with each other via stress superposition and reduction. The shear stresses on the middle or interior hydraulic fractures are still symmetric. However, the shear stresses on both sides of the outmost hydraulic fractures are asymmetric, which changes the local principal stress's direction and then promotes the turning of the outmost hydraulic fractures. Consequently, the interior and middle hydraulic fractures propagate planarly, but the outmost hydraulic fractures present significant deflection in the 3D morphology, as shown in Fig. 6. Also, the shear stress distribution in the XY section is much more uniform than that in the XZ section because of the existence of soft layers in the height growth direction (Z-axis).

3.2. Simultaneous propagation behaviour of multiple hydraulic fractures in layered tight reservoirs

Once the middle and interior hydraulic fractures are stagnated, the hydraulic fracture propagation in one fracturing stage only is localised at the outmost hydraulic fractures because of no constraint on their growth from outside the array. To further explore the interaction among multiple hydraulic fractures, the variations of fluid pressure at perforation clusters' mouths, flow
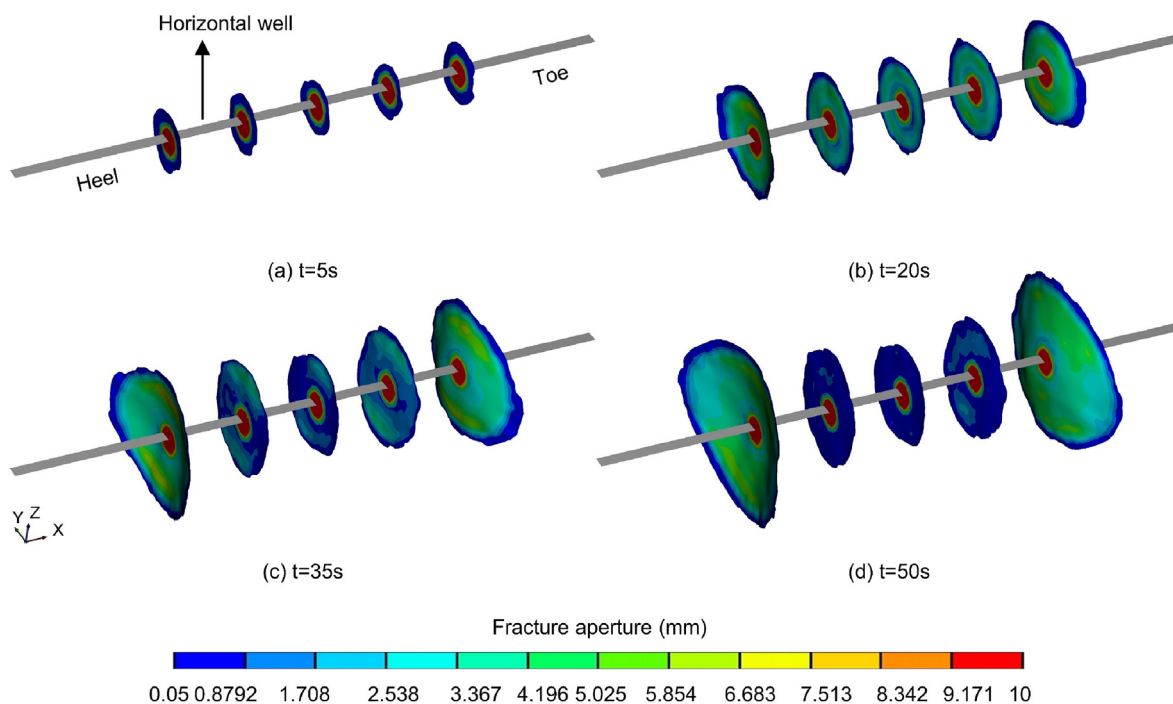
Fig. 6. Fracture morphology and aperture evolutions of multiple hydraulic fractures in the layered tight reservoir. Figures (a)–(d) cover the same region and are viewed from the same angle.

rates into perforation cluster, and fracture widths at the intersection points of perforation clusters and horizontal well are illustrated in Fig. 8. It can be seen from Fig. 8(a) that the injection pressures are almost the same across all perforation clusters due to the fluid pressure continuity along the horizontal well. Note that if the friction of horizontal well is considered, the injection pressure at each intersection point will be different due to the pressure loss. At the beginning of fluid injection, the injection pressure increases rapidly due to the storage of fracturing fluid in the initial hydraulic fractures. After that, the injection pressure decreases monotonically and finally remains constant at the stable propagation stage with a value around 47.3 MPa.

Flow rate into each perforation cluster is presented in Fig. 8(b), denoting the amount of fracturing fluid receiving by each perforation cluster. As shown in Fig. 8(b), at the early stage of hydraulic fracture propagation, all perforation clusters receive the same amount of fracturing fluid with a flow rate equal to 0.004 m^3/s. After that, the outmost perforation clusters take more and more fracturing fluid, while the flow rates in the middle and interior perforation clusters gradually decrease to 0 m^3/s. More specifically, the middle perforation cluster stop receiving fracturing fluid at 22.4 s, while the 4th and 2nd perforation clusters no longer take fracturing fluid at 29.4 s and 34.4 s, respectively. The stress shadow effect discussed in the previous section can be used to explain the uneven flow rate distribution. For example, the middle hydraulic fracture is constrained by the interior hydraulic fractures first due to the formation of compressional stress at the fracture tip, which significantly increases its flow resistance for further propagation. Similarly, the interior hydraulic fractures' flow resistance increases due to the stress shadow induced by the outmost hydraulic fractures' propagation. As a result, the outmost perforation clusters have the smallest flow resistance. The fracturing fluid prefer flowing into the perforation cluster with the least flow resistance to minimize the energy consumption of the whole physical process. Once the perforation cluster stops taking fracturing fluid, its growth

will be stunted soon, as shown in Fig. 5. The growth of the 2nd, 3rd, and 4th perforation clusters stagnates at the time of 38 s, 28 s, and 40 s, respectively. As a result, the growth of the middle hydraulic fracture is minimal. The fluctuations on the time evolution curves of flow rate illustrate the dynamic disturbance to the local stress filed and strong interference among multiple hydraulic fractures during the pumping.

The time evolution of the fracture width at the intersection points between the perforation clusters and horizontal well is plotted in Fig. 8(c). From this plot, it is found that the fracture width of intersection points performs identically and follows the variation of injection pressure at the beginning of fluid injection. Then, as the stress shadow effect becomes dominant, the middle and interior perforation clusters take lesser fracturing fluid and subject to the compressive stress adjacent to fracture opening, resulting in the suppression on their intersection points. On the contrary, the fracture width at the intersection points of the outmost perforation clusters increases with time due to the inside fracturing fluid pressure higher than the surrounding compressive stress.

Fig. 8(d) plots the time evolution of fracture tip extent in the length (Y-axis) and height (Z-axis) directions, where the sign represents the extent in positive or negative direction of the axes. Since the middle and interior hydraulic fractures lag behind the outmost hydraulic fractures and stagnate soon after injection starting as illustrated in Fig. 6, only the extent of outmost hydraulic fractures is plotted in Fig. 8(d). From this plot, one can see that the fracture tip extent equally increases in the height and length directions in the first 10 s, denoting the radial growth of the outmost hydraulic fractures during this period. Lather, the growth of the length exceeds that of the height, resulting in the elliptic shape of hydraulic fractures. Another conclusion can be obtained from Fig. 8(d) is that even though the outmost hydraulic fractures are placed symmetrically, their growths are asymmetric and do not develop at the same rate. For example, the maximum fracture length extent is observed in the 5th hydraulic fracture with a value of +10.77 m,
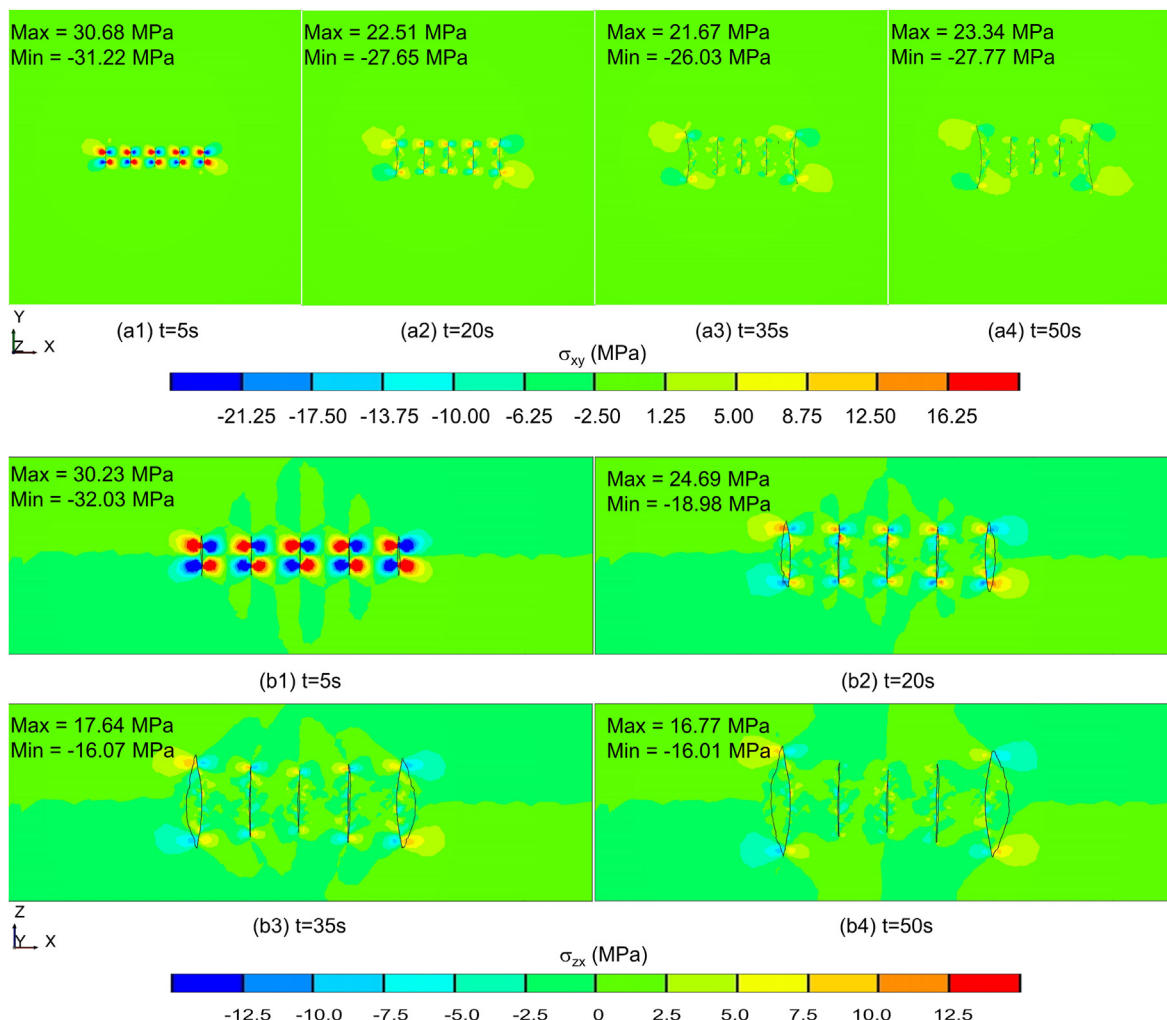
Fig. 7. Shear stress evolutions at the middle XY and XZ sections of the layered tight reservoir during the simultaneous growth of multiple hydraulic fractures. Compared with the XY sections, the XZ sections are zoomed-in twice for a better illustration.

while the minimum fracture length extent is observed in the 1st hydraulic fracture with a value of -13.16 m. Both the maximum and minimum fracture extents in the height direction occur in the 1st hydraulic fracture and equal $+7.72$ m and -7.42 m, respectively. The reason behind this may be due to the flow resistance's difference between the 1st and 5th hydraulic fractures induced by different stress shadows.

3.3. Parametric study on the layered modulus effect

Another three simulations are carried out to evaluate the effect of the soft layer's modulus on the simultaneous propagation of multiple hydraulic fractures in layered tight reservoirs, by changing the soft layer's modulus from 16 GPa to 24 GPa, 8 GPa, and 4 GPa, respectively. The propagation behaviours of these three reservoirs overall are similar to that in the reservoir with a soft layer's modulus of 16 GPa. For example, the interior and middle hydraulic fractures are suppressed by the preferential growth of the outmost hydraulic fractures. Therefore, only the final hydraulic fracture networks created in these four reservoirs are compared in Fig. 9, including 3D fracture pattern, total fracture length, and total

fracture height. The magnitudes of the local fracture aperture with a colour bar are used to colour the hydraulic fractures. In the plot, the first, second, third, and fourth columns correspond to the soft layer's modulus equal to 24 GPa, 16 GPa, 8 GPa and 4 GPa, respectively.

It can be seen from Fig. 9(a1-a4) that the growth mainly localises on the two outmost hydraulic fractures that have a larger fracture height and length than the middle and interior hydraulic fractures, regardless of the soft layer's modulus. It is worth mentioning that the middle and interior hydraulic fractures always stop their height growth in the soft layers. The middle and interior hydraulic fractures are also compressed to the minimum fracture aperture at the position outside the initial hydraulic fracture. Note that the fracture aperture for the initial hydraulic fracture is 10 mm, while that for the newly created hydraulic fracture has a minimum value of 0.05 mm. Fig. 9(a1-a4) also shows that the young's modulus of soft layer has an apparent effect on the final hydraulic fracture pattern, especially on that of the outmost hydraulic fractures. With the decrease of the soft layer's modulus, the containment effect of soft layer in the height direction strengthens. In consequence, the length growth has become the preferred direction of hydraulic
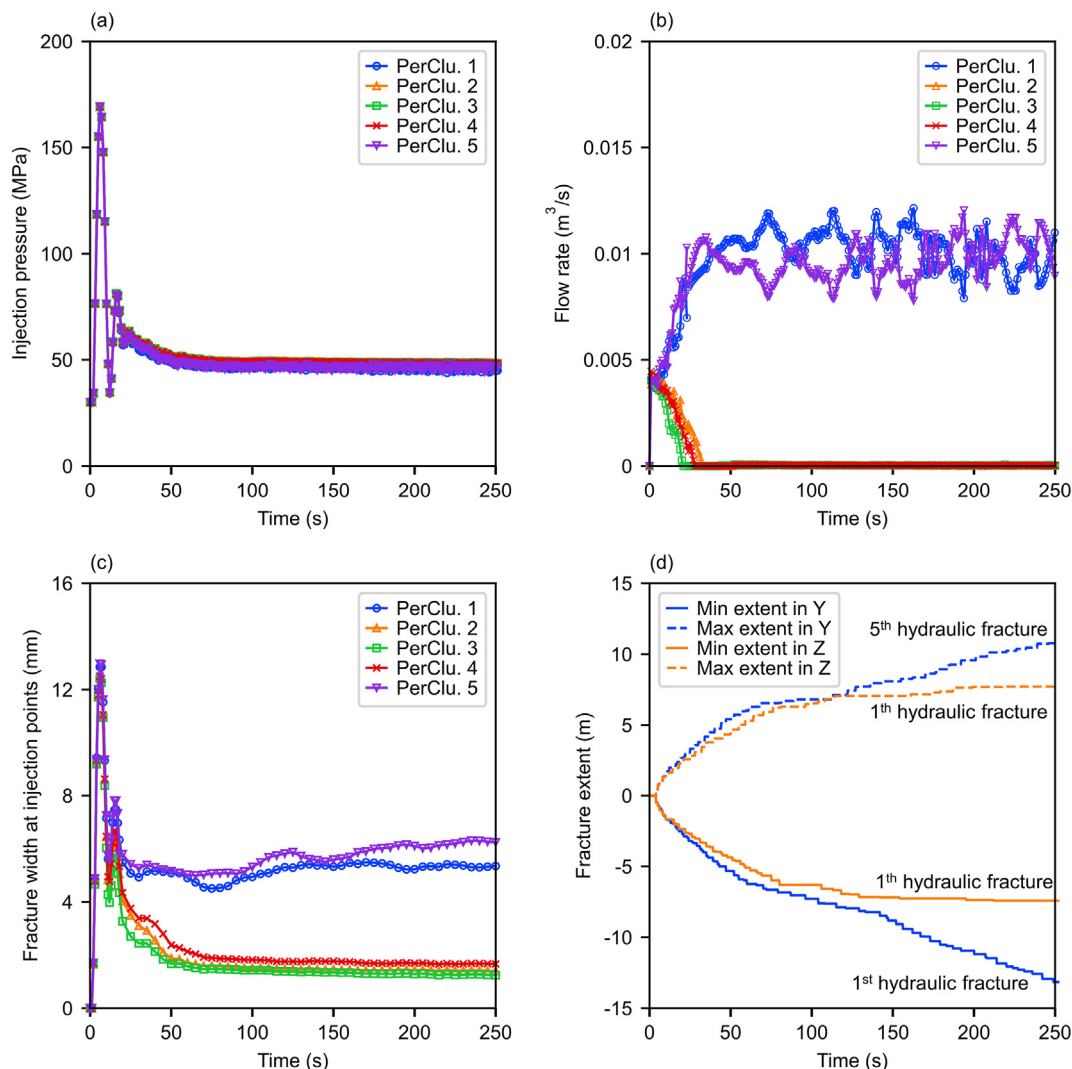
Fig. 8. Variations of (a) injection pressure, (b) flow rate, and (c) fracture width at the injection point of each perforation cluster in the layered tight reservoir. The subfigure (d) shows the fracture tip extent in different directions, and the negative (or positive) magnitude means the extent in negative (or positive) direction of the axis. PerClu in subfigures (a)–(c) is the abbreviation of perforation cluster.
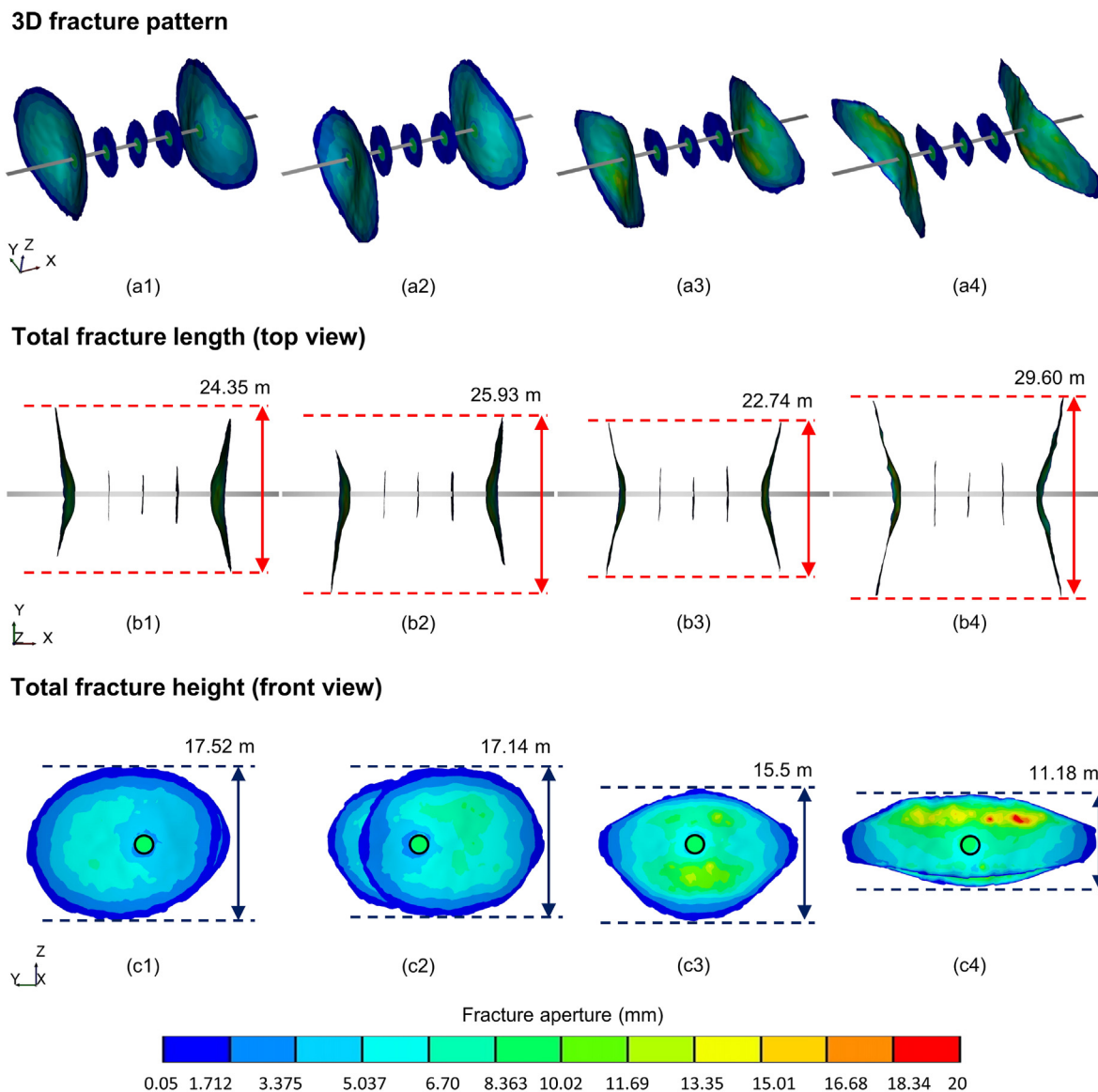
fracture propagation, and the height growth of each hydraulic fracture decreases. The deflection and curving of the outer hydraulic fractures intensify with the reduction of soft layer's modulus. The shape of the middle and interior hydraulic fractures changes from the elliptic type with the major axis in the height direction to the blade-like type with the major axis in the length direction, as the soft layer's modulus decreases.

Since the middle and interior hydraulic fractures are inhibited in their growth, their contributions to the hydrocarbon recovery are limited. The stimulated extent, e.g., fracture length, height, area, and volume, of the created hydraulic fracture network in one fracturing stage depends on the geometry of the outmost hydraulic fractures. In Fig. 9(b1-b4), one can see that the fracture patterns of symmetrically placed hydraulic fractures, e.g., the 1st and 5th perforation clusters or the 2nd and 4th perforation clusters, becomes more symmetric overall with the decline of soft layer's modulus. For a single hydraulic fracture, its fracture length extent also becomes more symmetrically on the two sides of the horizontal well due to the change of propagation type from single-wing to bi-wing, as the soft layer's modulus decreases. The fracture length extent in the layered reservoir with a soft layer's modulus of

4 GPa is the largest, while the shortest fracture length extent is observed in the layered reservoir with a soft layer's modulus of 8 GPa. The layered tight reservoirs with soft layer's moduli of 24 GPa and 16 GPa have relatively larger total fracture lengths due to their single-wing propagation in the outmost hydraulic fractures.

Fig. 9(c1-c4) plots the total fracture height variation, illustrating that the total fracture height decreases apparently with the decrease of soft layer's modulus. The total fracture height extent in the fracturing stage decreases from 17.52 m to 11.18 m, as the soft layer's modulus in the layered reservoir decreases from 24 GPa to 4 GPa. The outmost hydraulic fractures prefer growing in single-wing type in the height direction when the layer reservoir has a lower soft layer's modulus. For example, the outmost hydraulic fractures prefer growing in the negative Z direction in the layered reservoir with a soft layer's modulus of 8 GPa but tend to propagate in the positive Z direction in the layered reservoir with a soft layer's modulus of 4 GPa. However, the outmost hydraulic fractures propagate a bit more uniformly into bi-wing on the two sides of horizontal well in the layered reservoirs with soft layer's moduli of 24 GPa and 16 GPa.

In addition, the overall local fracture aperture distribution in the

3D fracture pattern

Total fracture length (top view)

Total fracture height (front view)

Fracture aperture (mm)

0.05 1.712 3.375 5.037 6.70 8.363 10.02 11.69 13.35 15.01 16.68 18.34 20

Fig. 9. Comparison of created three-dimensional hydraulic fracture networks in layered tight reservoirs with a soft layer's modulus of 24 GPa (1st column), 16 GPa (2nd column), 8 GPa (3rd column), and 4 GPa (4th column). The hydraulic fractures are coloured with the magnitude of local fracture aperture. In each row, the subplots are snapshot from the same region and angle.

outmost hydraulic fractures increases clearly with the decrease of soft layer's modulus, as shown in Fig. 9(d1-d4). For a given reservoir, the region with larger fracture apertures is mainly located in the soft layer, while the local fracture aperture in the stiff layer is smaller. This is because the hydraulic fracture propagation in the stiff layer attracts larger stress intensity at the fracture tip and thus produces smaller aperture. Since the outmost hydraulic fractures consume most of the fracturing fluid, the total fracture area created by the array of five perforation clusters is mainly attributed to the outmost hydraulic fractures. The narrower fracture aperture benefits the propagation and extension of hydraulic fractures. Consequently, the total fracture area in the layered reservoirs increases with decreasing the soft layer's modulus, as shown in Fig. 10(a). The fracturing fluid leak-off is proportional to the fracture area, and thus, the leak-off volume is also higher in the layered reservoir with a higher soft layer's modulus, as shown in Fig. 10 (b). Due to the requirement for mass/volume conversation, the more fracturing fluid leaks into the reservoir, the lesser hydraulic fractures volume

is created to preserve the remaining fluid. Fig. 10(c) shows that the created hydraulic fracture volume increases, as the soft layer's modulus decreases.

The fracture pattern plotted in Fig. 9 shows that the outmost perforation clusters eventually take all the fracturing fluid and present dominant fracture growth, regardless of the soft layer's modulus. Here, how the soft layer's modulus influences the flow rates into middle and interior perforation clusters is examined and shown in Fig. 11. From Fig. 11, one can see that the middle perforation cluster (PerfClu. 3) always stops accepting fracturing fluid in the first place compared with other perforation clusters, and consequently, its growth is minimal in all the layered tight reservoirs. The time that the middle perforation cluster stops the uptake of fluid flux is earlier in the layered tight reservoir with a smaller soft layer's modulus. It is interesting to note that even though the 2nd and 4th perforation clusters are placed symmetrically along the horizontal well, their time evolutions of flow rate are different, denoting that they are subjected to different stress shadow effects.
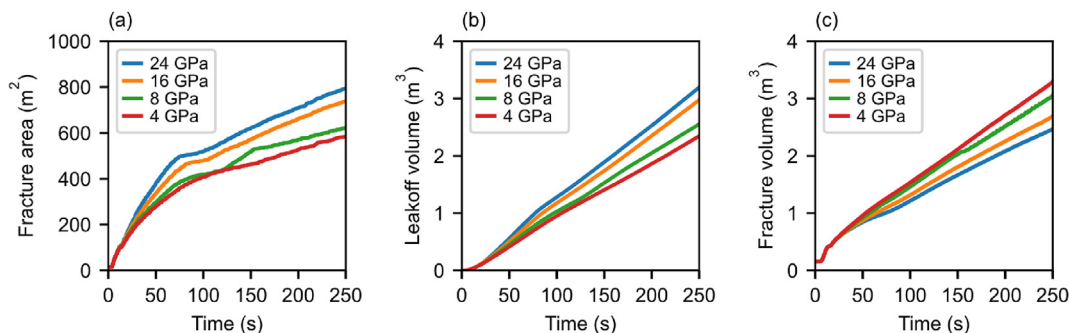
Fig. 10. Time evolutions of (a) total fracture area, (b) total leak-off volume, and (c) total hydraulic fracture volume in layered tight reservoirs with various soft layer's moduli.
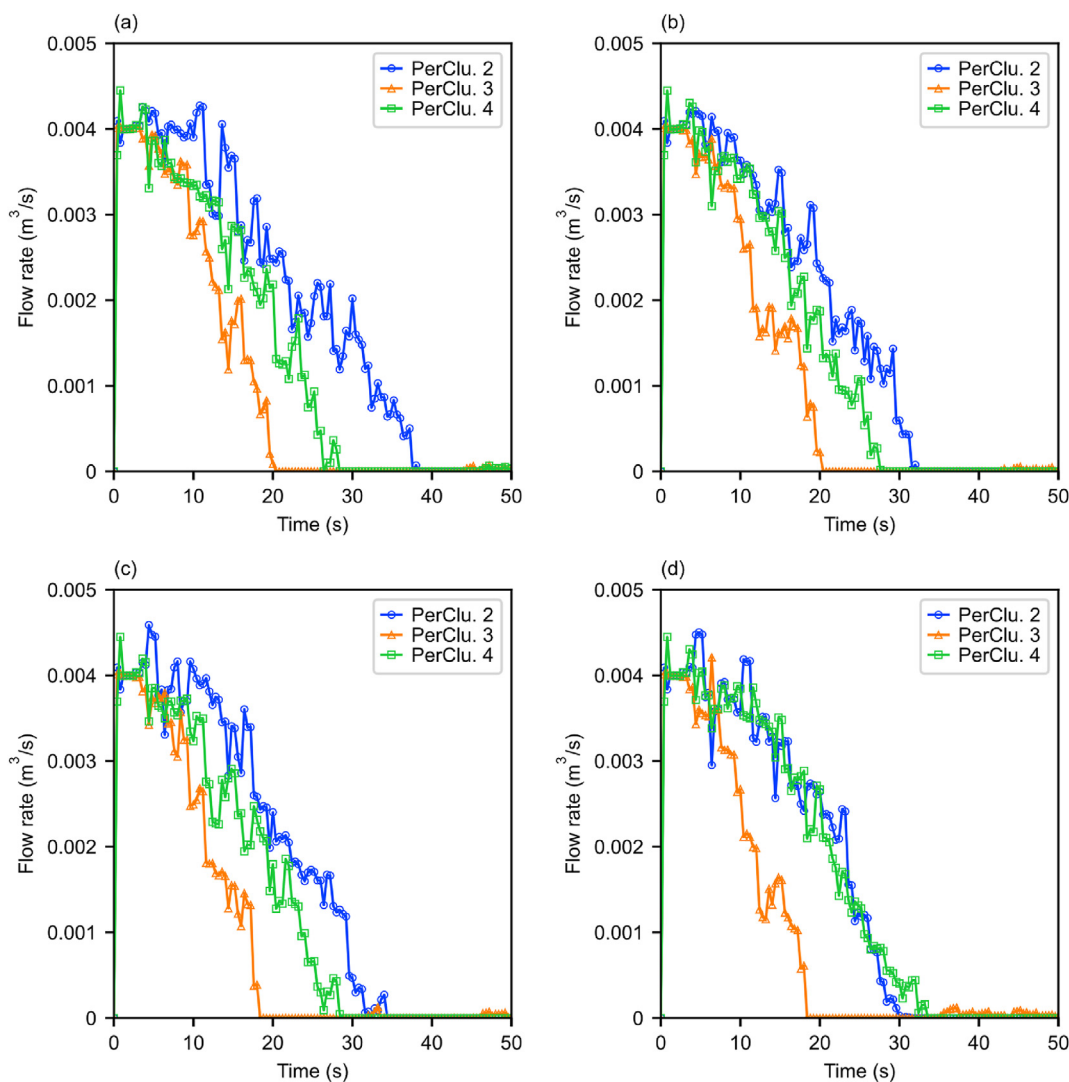

Fig. 11. Time evolution of flow rates in the middle (PerClu. 3) and interior (PerClu. 2 and PerClu. 4) perforation clusters of layered reservoirs with a soft layer's modulus of (a) 24 GPa, (b) 16 GPa, (c) 8 GPa and (d) 4 GPa. PerClu is the abbreviation of perforation cluster.

As the soft layer's modulus decreases, the time that stops accepting fracturing fluid of the 2nd perforation cluster decreases, but that of the 4th perforation cluster increases. When the soft layer's modulus decreases to 4 GPa, the flow rate distributions of the 2nd and 4th perforation clusters are very close to each other, leading to the symmetric fracture pattern of the interior hydraulic fractures in

Fig. 9(a4). Remember that the outmost hydraulic fractures in the layered reservoir with a soft layer's modulus of 4 GPa is also more symmetric compared with other cases. Therefore, one can expect a more symmetric fracture pattern and flow rate distribution in an array of perforation clusters placed in a layered tight reservoir with a smaller soft layer's modulus.

3.4. Effect of fracturing fluid leak-off, perforation number and flow rate distributions

The effects of the fracturing fluid leakage, perforation number, and flow rate distribution on the simultaneous propagation behaviour of multiple hydraulic fractures in layered tight reservoirs with a soft layer's modulus of 16 GPa are evaluated in this section. It is worth mentioning that the model uses the same parameters as those listed in Table 1 − Table 3 without specification.

Fig. 12 compares the final fracture patterns obtained from the layered tight reservoirs with three different leakage coefficients, i.e., 5×10^{-4} m/s$^{0.5}$, 1×10^{-4} m/s$^{0.5}$, 0 m/s$^{0.5}$. In Fig. 12(a−c), one can see that the fracturing fluid leakage has an insignificant effect on the simultaneous propagation of an array of multiple perforation clusters, since the preferential growth is always observed on the outmost hydraulic fractures. Fig. 12(a−c) also shows that the local fracture aperture distribution increases with the decrease of the leakage coefficient. The leakage coefficient influences the created fracture area substantially, as shown in Fig. 12(d). Fig. 12(d) also illustrates that the leakage coefficient has a minor effect on the fracture area evolution at the beginning of the fluid injection since

the fracturing fluid leak-off is determined by the intrinsic permeability of the layered tight reservoir at the start, as stated in Section 2.2.

The effect of perforation number on the simultaneous growth of multiple hydraulic fractures in layered tight reservoirs is illustrated in Fig. 13. Fig. 13(a−c) corresponds to the final fracture pattern obtained from the layered tight reservoirs with 0, 4, and 8 perforations in every cluster. 0 perforation means no perforation pressure drop technique is used in the 3D multi-cluster fracturing. Fig. 13(a−c) shows that the growths of the middle and interior hydraulic fractures are always compressed by the outmost hydraulic fractures, regardless of the number of perforations. As the perforation number of every cluster increases, the created total fracture area in the layered tight reservoir decreases, as shown in Fig. 13 (d). For example, the total fracture area created in the layered tight reservoir is 745.866 m^2, 739.945 m^2, and 695.57 m^2 when the perforation number in every cluster is 0, 4 and 8, respectively. In consequence, the total leak-off volume decreases with the increasing perforation number, but the total fracture volume increases, as shown in Fig. 13(d) and (e).

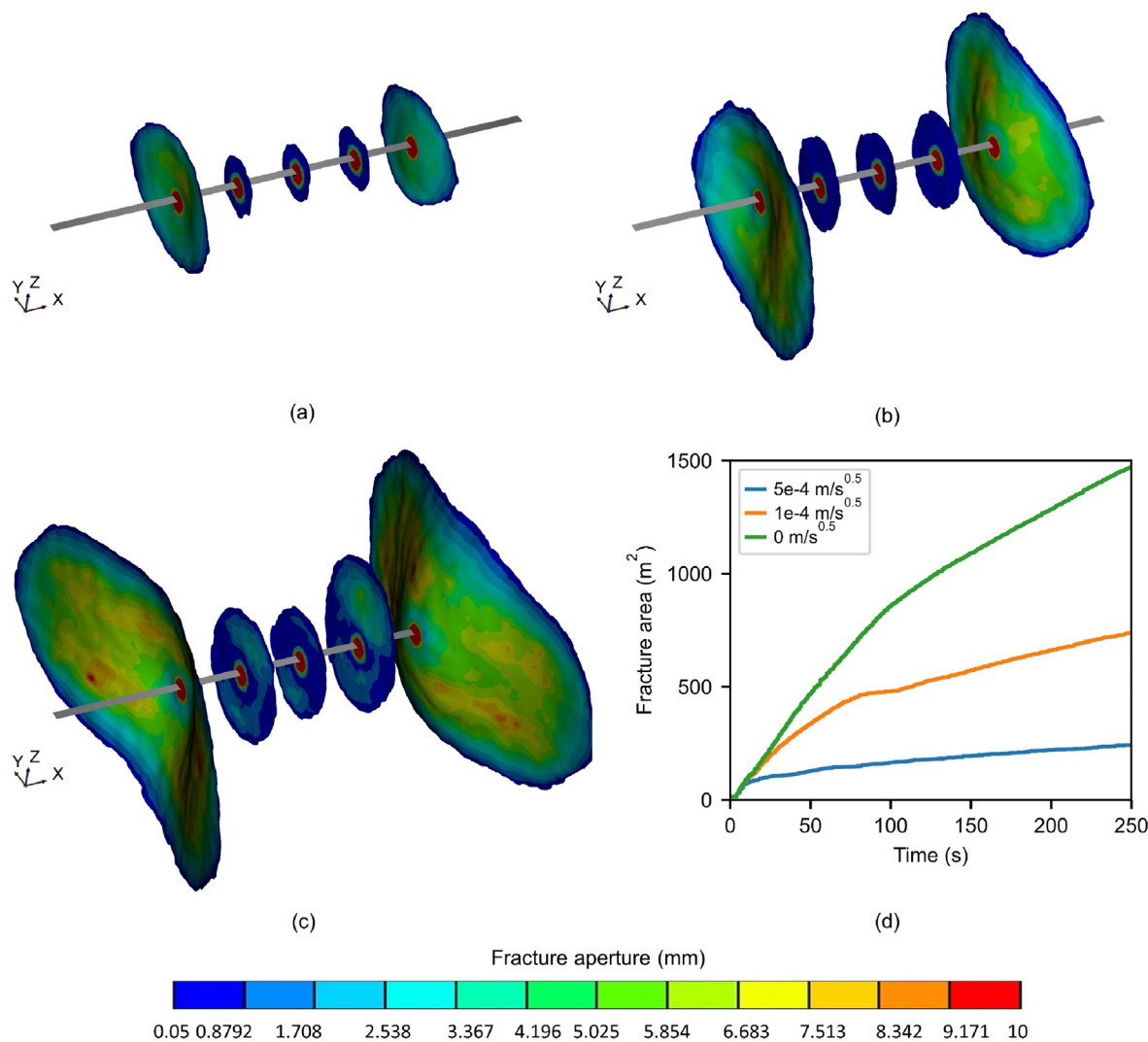In many previous 3D multi-cluster fracturing simulations, the

(a)

(b)

(c)

(d)

Fracture aperture (mm)

0.05 0.8792 1.708 2.538 3.367 4.196 5.025 5.854 6.683 7.513 8.342 9.171 10

Fig. 12. Comparison of the created final fracture patterns in layered tight reservoirs with a leak-off coefficient of (a) 5×10^{-4} m/s$^{0.5}$, (b) 1×10^{-4} m/s$^{0.5}$, and (c) 0 m/s$^{0.5}$. (d) The evolutions of total fracture area created in the layered tight reservoirs with different leak-off coefficients. The hydraulic fractures are coloured with the magnitude of local fracture aperture, and they are snapshots under the same region and angle.
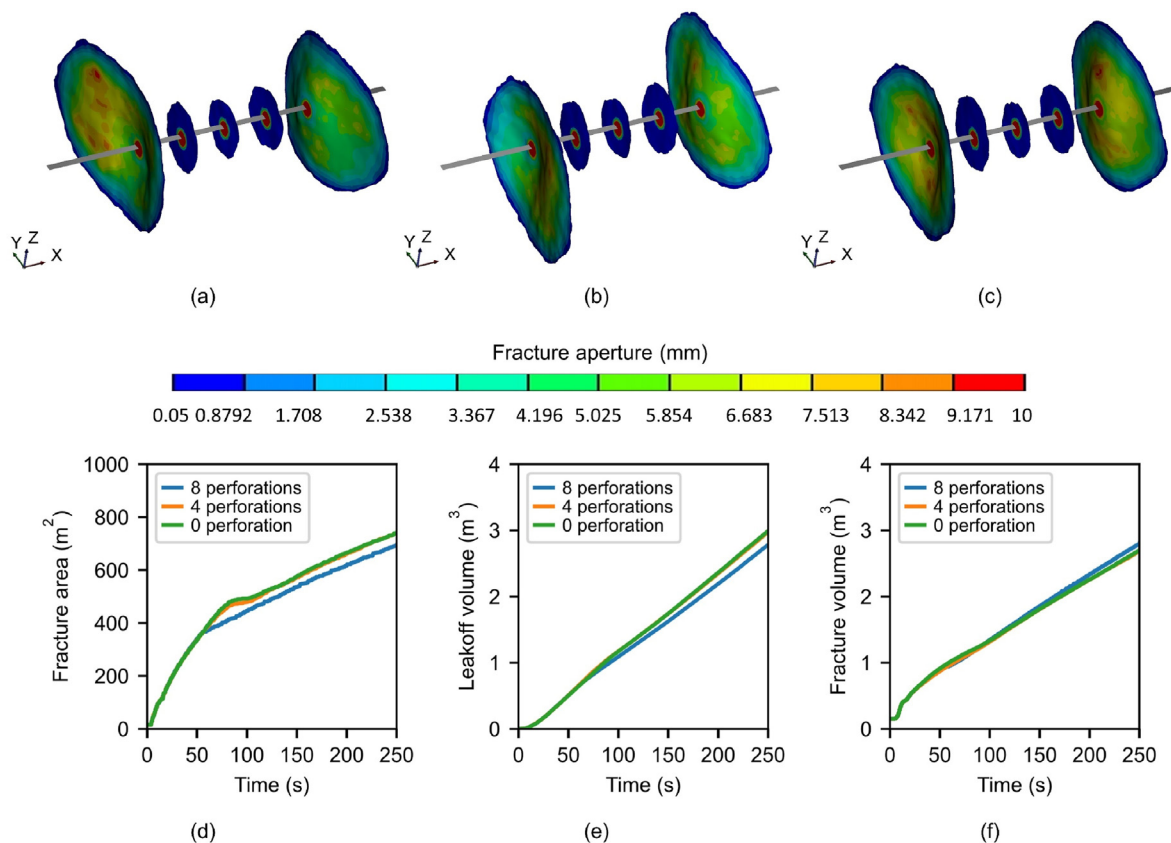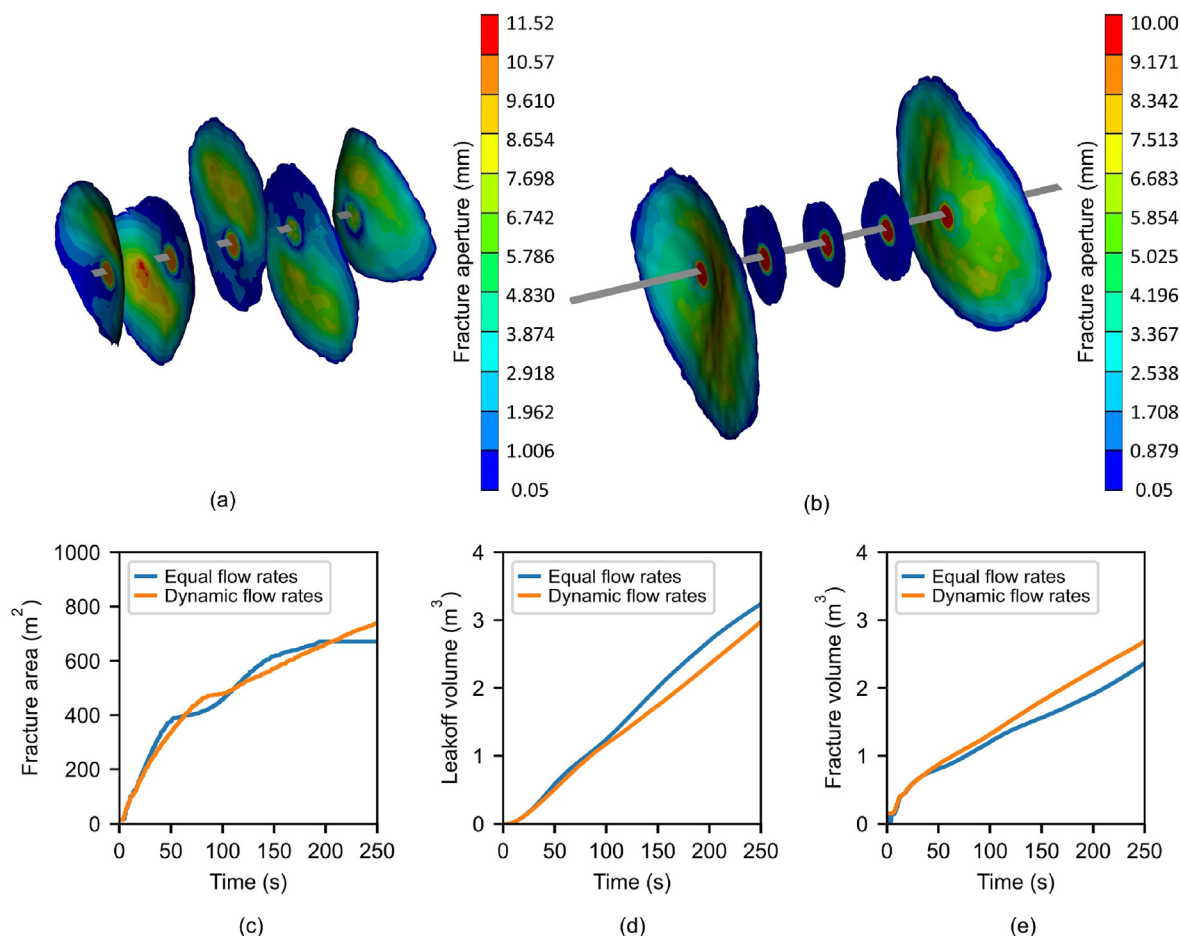
Fig. 13. Comparison of the created final fracture patterns in layered tight reservoirs with a perforation number of (a) 0, (b) 4, and (c) 8 in every perforation cluster. The evolutions of (d) total fracture area, (e) total leak-off volume and (f) total fracture volume created in the layered tight reservoirs with different peroration numbers in every cluster. The hydraulic fractures are coloured with the magnitude of local fracture aperture, and they are snapshots under the same region and angle.

equal flow rate was often used in every perforation cluster for simplification [17]. Such an approach does not require the establishment of horizontal well and indeed violates the fluid pressure continuity along the horizontal well and the dynamic flow rate distributions among perforation clusters in practice. Here, the fracture patterns obtained from the layered tight reservoirs stimulated by using dynamic and equal flow rates among perforation clusters are compared. Note that the equal flow rate distribution is achieved by using a single horizontal well in every initial perforation cluster, and every horizontal well has the same flow rate of 0.004 m³/s. The final fracture patterns created by the equal and dynamic flow rate distributions are illustrated in Fig. 14(a) and Fig. 14(b), respectively. From these two plots, it is found that the simultaneous growth of multiple hydraulic fractures is much more uniform in the layered tight reservoir stimulated by using the equal flow rate strategy. In other words, the violation of the fluid pressure continuity by without considering the dynamic flow rate distributions overestimates the growth of the interior and middle hydraulic fractures. Fig. 14(c) illustrates that the dynamic flow rate distributions among perforation clusters contribute a larger total fracture area than the equal flow rate distributions. The reason is that the multiple hydraulic fractures driven by the equal flow rate distributions stop extending at t = 195 s because of their strong competition, and after that, the injected fracturing fluid is mainly used to increase the fracture aperture and leak into the reservoir. As a result, the layered tight reservoir stimulated by the equal flow rate distributions has a larger total leak-off volume but a smaller total fracture leak-off volume than that stimulated by the dynamic flow rate distributions, as shown in Fig. 14(d) and (e).

3.5. Discussion

The results obtained from this study illustrate the similar simultaneous developments of an array of multiple perforation clusters in layered tight reservoirs, regardless of the soft layer's modulus. Overall, the outmost hydraulic fractures grow dominantly, while the middle and interior hydraulic fractures are substantially suppressed. The mechanism behind is related to the stress shadow effect during the hydraulic fracture propagation. The additional compressional stress induced by the outmost hydraulic fractures on the interior and middle hydraulic fractures increase their flow resistance, which favours fracturing fluid flow into the outmost perforation clusters. As a result, the new fracturing area within a fracturing stage is mainly created by expanding the two outmost hydraulic fractures, whereas the fracturing area growth in the interior and middle hydraulic fractures is very limited and makes little contribution to the hydrocarbon stimulation.

In order to promote the uniform flow rate distribution in the array of perforation clusters and then ensure the fracture propagation from all clusters within a fracturing stage, nonuniform cluster spacing and limited entry design techniques are often recommended. The former method aims at relieving the mechanical interactions in the array of hydraulic fractures by reducing the spacing between interior perforation clusters and outmost perforation clusters, e.g., moving 2nd and 4th clusters away from each other and towards the 1st and 5th clusters, respectively. The latter method is to introduce different peroration pressure drops into clusters by adjusting their perforation number/diameter accordingly. For example, one can increase the perforation pressure drop
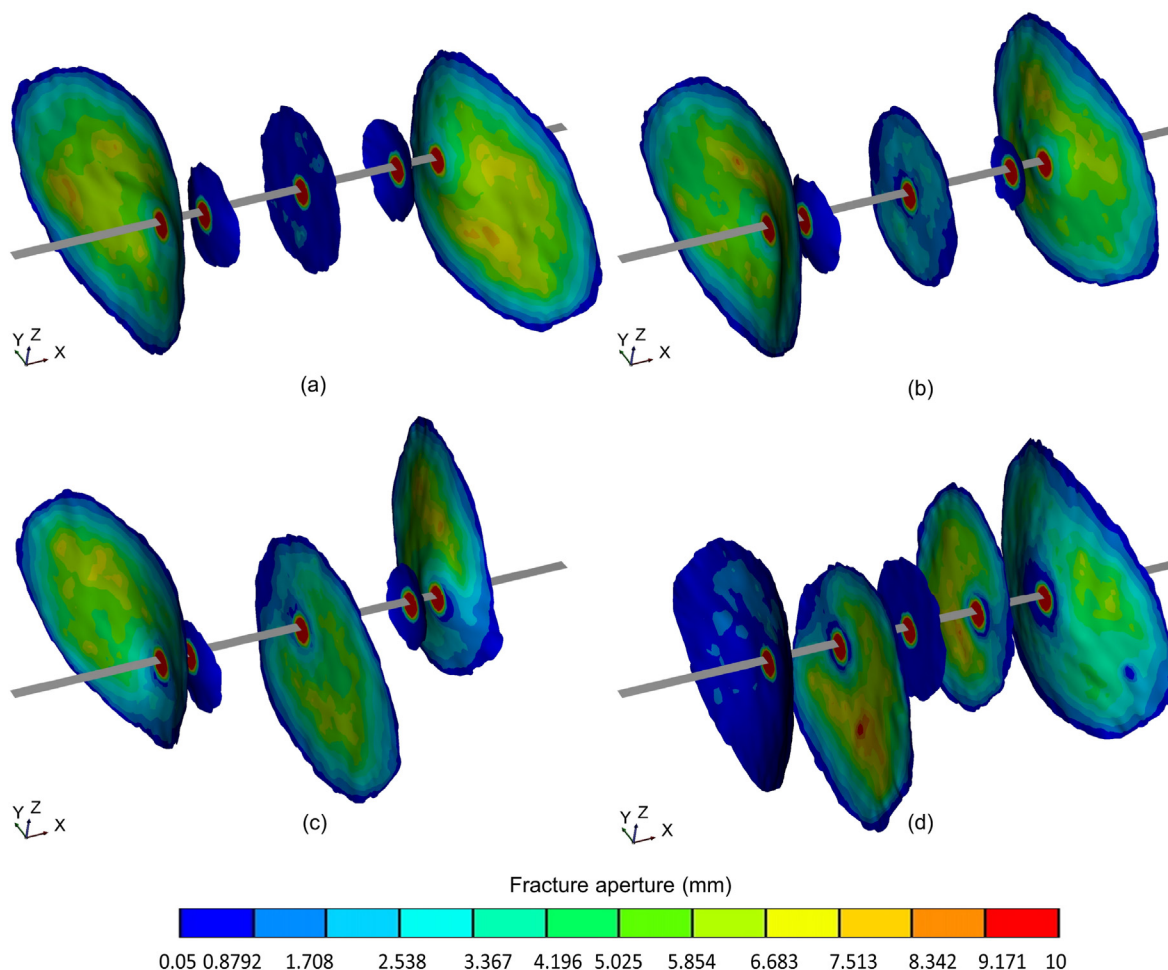
Fig. 14. The final fracture pattern obtained from the layered tight reservoir stimulated by the (a) equal and (b) dynamic flow rate distributions. The comparison of the evolutions of (c) total fracture area, (d) total leak-off volume and (e) total fracture volume in the layered tight reservoirs stimulated by the dynamic and equal flow rate distributions. The hydraulic fractures in (a) and (b) are coloured with the magnitude of local fracture aperture, and they are snapshots under the same region and angle.

of the two outmost clusters by decreasing their perforation numbers/diameters or reduce the perforation pressure drop of the middle and interior clusters by increasing their perforation numbers/diameters. Through these two methods, the middle and interior clusters' flow resistances can be reduced, letting them accept more fracturing fluid and then promoting their growth. The efficiencies of these two methods have been proven numerically by using planar or constant-height 3D models [9,18,47]. These 3D models restrict the potential non-planar (e.g., curving and deflection) behaviour and/or height variation of hydraulic fractures and neglect the effects of leak-off and layering structure. The performance of these two methods in the non-planar 3D simulation considering leak-off and layering structures remains unclear.

Here, the performance of nonuniform cluster spacing in the layered tight reservoir with a soft layer's modulus of 16 GPa is investigated by using Elfen TGR. As suggested by Peirce and Bunger [8] and Wu et al. [41], the 2nd and 4th clusters are moved away from each other and towards the 1st and 5th clusters, respectively. Three cases of nonuniform cluster spacings are considered herein: (i) the spacing between every two adjacent cluster equal to 3 m (1st and 2nd), 7 m (2nd and 3rd), 7 m (3rd and 4th), and 3 m (4th and 5th); (ii) the spacing between every two adjacent clusters equal to 2.5 m (1st and 2nd), 7.5 m (2nd and 3rd), 7.5 m (3rd and 4th), and 2.5 m (4th and 5th); and (iii) the spacing between every two adjacent clusters equal to 2 m (1st and 2nd), 8 m (2nd and 3rd), 8 m (3rd and 4th), and 2 m (4th and 5th). The final fracture patterns obtained

from these three cases are illustrated in Fig. 15(a−c), respectively. From Fig. 15(a−c) and Fig. 9(a2), one can see that, as the spacing between interior and outmost clusters reduces, the interior hydraulic fractures are suppressed more significantly, and the dominant growth can also be found in the middle hydraulic fracture. The total fracture areas generated by nonuniformly spaced clusters are 776.23 m², 753.38 m², and 742.18 m² in Fig. 15(a−c), respectively, while the fracture area generated by uniformly spaced clusters in Fig. 9(a2) is 739.95 m². Note that 776.23 m² is almost the maximum value of total fracture area that can be achieved by nonuniformly spaced clusters through trial and error, which is only 5% higher than the total fracture area generated by the uniformly spaced clusters. However, the planar 3D simulation results of Peirce and Bunger [8] showed that the nonunifrom cluster spacing could achieve a more uniform growth of hydraulic fractures among the five perforatrion clusters, and it increased the total fracture area in the stage by 46% compared with the uniform clsuter spacing. This difference suggests that the non-uniform cluster spacing approach may not efficiently promote the non-planar simultaneous hydraulic-fracture growth in tight reservoirs with fluid leak-off and layered structures.

The authors discover that the adjustment of pumping rate is more effective than the nonuniform cluster spacing in promoting the simultaneous growth of multiple hydraulic fractures in layered tight reservoirs. For example, Fig. 15(d) is the final fracture pattern created by the uniformly spaced clusters in the layered tight reservoir with a soft layer's modulus of 16 GPa, a pumping rate of

Fracture aperture (mm)

0.05 0.8792 1.708 2.538 3.367 4.196 5.025 5.854 6.683 7.513 8.342 9.171 10

Fig. 15. (a)−(c) compare the final fracture patterns obtained from layered tight reservoirs with different nonuniform cluster spacings. Along the positive direction of x-axis, the spacing between every two adjacent clusters equals (a) 3 m, 7 m, 7 m, and 3 m, (b) 2.5 m, 7.5 m, 7.5 m, and 2.5 m, and (c) 2 m, 8 m, 8 m, and 2 m. (d) illustrates the final fracture pattern obtained from the layered tight reservoir with a uniform cluster spacing of 5 m and a pumping rate of 0.03 m³/s. The hydraulic fractures are coloured with the magnitude of local fracture aperture. Here the fracture patterns are snapshot under the same region and angle as that in Fig. 7(a1-a4) but are zoomed-in twice for a better presentation.

0.03 m^3/s, and a pumping volume of 5 m^3. Compared with the final fracture pattern in Fig. 9(a2) and Fig. 15(a−c) where the pumping rate is 0.02 m^3/s, the distribution of fracture surface across the fractures in the stage is much more uniform in Fig. 15(d). Although the middle hydraulic fracture is still suppressed, the outmost and interior hydraulic fractures propagate dominantly, as shown in Fig. 15(d). In consequence, the total fracture area in Fig. 15(d) reaches 1063.07 m^2, which is 43.6% and 37.0% higher than that in Fig. 9(a2) and Fig. 15(a), respectively. However, it is worth mentioning that a higher injection rate requires more energy to pump the fracturing fluid. Whether a higher pumping rate always promotes the simultaneous growth and generates a larger total fracture area will be investigated in the coming work.

4. Conclusions

The hydromechanical coupled FDEM is employed in this study to investigate the simultaneous hydraulic-fracture growth in the layered tight reservoirs. In the hydromechanical model, the non-planar 3D growth of hydraulic fractures, dynamic flow rate distribution among clusters, perforation friction, pressure equilibrium along the horizontal well, and fracturing fluid leak-off are considered. The simultaneous propagation behaviour and mechanism of

hydraulic fractures from an array of five perforation clusters in the layered tight reservoir with alternating stiff and soft layers are investigated. In addition, the layered modulus effect on the simultaneous growth of multiple hydraulic fractures in terms of fracture pattern, fracture geometry (e.g., height, length, aperture, area, and volume), leak-off, dynamic flow rate partitioning has been explored by varying the soft layer's modulus. The effects of fracturing fluid leak-off, perforation friction and flow rate distribution are also investigated.

The simulation results show that, the dominant growth is always localised on the outmost hydraulic fractures, while the growths of the middle and interior hydraulic fractures are suppressed substantially. In particular, the middle and interior hydraulic fractures are compressed to the minimum aperture and stop their height growths at soft layers. The maximum principal stress evolution demonstrates the behind reason, that is, the stress shadow induced by the propagation of outmost hydraulic fractures exerts additional compression stress at the fracture tips of middle and interior hydraulic fractures. Consequently, the flow resistances in the middle and interior hydraulic fractures increase, leading the middle and interior perforation clusters to stop the uptake of fracturing fluid. The outmost hydraulic fractures propagate non-planarly and deflect significantly due to the asymmetric shear

stress distribution around their fracture tips, while the symmetric shear stress on both sides of middle and interior hydraulic fractures results in their planar growth.

Qualitative analysis of the layered modulus effect reveals that, with decreasing soft layer's modulus, the deflection and curving of the outmost hydraulic fractures intensify, while the shape of the compressed middle and interior hydraulic fractures changes from elliptic type with the major axis in the height direction to the blade-like type with the major axis in the length direction. The length growth of outmost hydraulic fractures prefers propagating into bi-wing, but its height growth tends to propagate into single-wing, as the soft layer's modulus decreases. The flow rate distributions in the two symmetrically placed hydraulic fractures, for example, the two interior/outmost fractures, are more consistent in a layered reservoir with a smaller soft layer's modulus, creating a more symmetric fracture pattern in the stage. Note that the middle perforation cluster always stops accepting the fracturing fluid at the first place, regardless of the soft layer's modulus.

The stimulated extent in the fracturing stage mainly depends on the fracturing region created by the outmost hydraulic fractures. Quantitative analysis on the layered modulus effect demonstrates that, as the soft layer's modulus decreases, the total fracture height in the stage decrease significantly, while the total fracture length overall increases. In addition, the local fracture aperture distribution on the outmost hydraulic fractures increases apparently with reducing the soft layer's modulus. As a result of this, for a given pumping volume of fracturing fluid, the total fracture area and the leak-off volume of fracturing fluid decrease, but the total fracture volume increases.

The numerical results present that the leak-off coefficient and perforation number have an insignificant effect on the simultaneous growth behaviour of multiple hydraulic fractures. The total fracture area decreases with the increasing leak-off coefficient and perforation number, but the total leak-off volume and total fracture volume increase. Violating the pressure continuity by without considering the dynamic flow rate distributions overrates the growth of middle and interior hydraulic fractures. The equal flow rate distribution produces smaller total fracture area and total fracture volume but a higher leak-off volume of fracturing fluid than the dynamic flow rate distribution in the layered tight reservoir, due to the strong competition among multiple hydraulic fractures.

It is also found that the nonuniform cluster spacing is not very effective in promoting the simultaneous hydraulic-fracture growth in layered tight reservoirs, and the total fracture area only increases by 5% compared with the uniform cluster spacing. Via increasing the pumping rate of uniformly spaced clusters slightly, the outmost and interior hydraulic fractures evolve dominantly, and the total fracture area is increased by 43.6%. Moreover, there are many important aspects related to layered tight reservoirs that deserve further study in the future work, e.g., the multi-stage fracturing, proppant transportation, effect of pumping rate, and shale gas production after hydraulic fracturing treatment.

Credit author statement

Lei Yang: Conceptualization, Methodology, Investigation, Formal analysis, Validation, Writing − original draft. **Shan Wu**: Methodology, Investigation, Writing − review & editing. **Ke Gao**: Methodology, Investigation, Resources, Writing − review & editing. **Luming Shen**: Conceptualization, Investigation, Writing − review & editing, Supervision, Funding acquisition.

Declaration of competing interest

The authors declare that they have no known competing financial interests or personal relationships that could have appeared to influence the work reported in this paper.

Acknowledgements

References

[1] Spence DA, Turcotte DL. Magma-driven propagation of cracks. J Geophys Res Solid Earth 1985;90(B1):575−80.

[2] Tsai VC, Rice JR. A model for turbulent hydraulic fracture and application to crack propagation at glacier beds. J Geophys Res: Earth Surf 2010;115(F3).

[3] Lecampion B, Bunger A, Zhang X. Numerical methods for hydraulic fracture propagation: a review of recent trends. J Nat Gas Sci Eng 2018;49:66−83.

[4] Liu Z, Pan Z, Li S, Zhang L, Wang F, Han L, et al. Study on the effect of cemented natural fractures on hydraulic fracture propagation in volcanic reservoirs. Energy 2022;241:122845.

[5] Chen X, Zhao J, Li Y, Yan W, Zhang X. Numerical simulation of simultaneous hydraulic fracture growth within a rock layer: implications for stimulation of low-permeability reservoirs. J Geophys Res Solid Earth 2019;124(12): 13227−49.

[6] He J, Li X, Yin C, Zhang Y, Lin C. Propagation and characterization of the micro cracks induced by hydraulic fracturing in shale. Energy 2020;191:116449.

[7] Dontsov EV, Suarez-Rivera R. Propagation of multiple hydraulic fractures in different regimes. Int J Rock Mech Min Sci 2020;128:104270.

[8] Bunger APP, Zhang X, Jeffrey RGG. Parameters affecting the interaction among closely spaced hydraulic fractures. SPE J 2012;17(1):292−306.

[9] Peirce APP, Bunger APP. Interference fracturing: nonuniform distributions of perforation clusters that promote simultaneous growth of multiple hydraulic fractures. SPE J 2014;20(2):384−95.

[10] Sobhaniaragh B, Mansur WJ, Peters FC. The role of stress interference in hydraulic fracturing of horizontal wells. Int J Rock Mech Min Sci 2018;106: 153−64.

[11] Zheng P, Xia Y, Yao T, Jiang X, Xiao P, He Z, et al. Formation mechanisms of hydraulic fracture network based on fracture interaction. Energy 2022;243: 123057.

[12] Middleton RS, Carey JW, Currier RP, Hyman JD, Kang Q, Karra S, et al. Shale gas and non-aqueous fracturing fluids: opportunities and challenges for super-critical CO2. Appl Energy 2015;147:500−9.

[13] Miller C, Waters G, Rylander E. Evaluation of production log data from horizontal wells drilled in organic shales. In: Presented at the North American unconventional gas Conference and Exhibition. The Woodlands, Texas, USA: Society of Petroleum Engineers; 2011.

[14] Spain DR, Gil I, Sebastian H, Smith PS, Wampler J, Cadwallader S, et al. Geo-engineered completion optimization: an integrated, multi-disciplinary approach to improve stimulation efficiency in unconventional shale reservoirs. In: SPE Middle East unconventional Resources Conference and Exhibition; 2015. D021S06R02.

[15] Lecampion B, Desroches J. Simultaneous initiation and growth of multiple radial hydraulic fractures from a horizontal wellbore. J Mech Phys Solid 2015;82:235−58.

[16] Tang H, Winterfeld PH, Wu Y-S, Huang Z-q, Di Y, Pan Z, et al. Integrated simulation of multi-stage hydraulic fracturing in unconventional reservoirs. J Nat Gas Sci Eng 2016;36:875−92.

[17] Salimzadeh S, Usui T, Paluszny A, Zimmerman RW. Finite element simulations of interactions between multiple hydraulic fractures in a poroelastic rock. Int J Rock Mech Min Sci 2017;99:9−20.

[18] Wu K, Olson JE. Mechanisms of simultaneous hydraulic-fracture propagation from multiple perforation clusters in horizontal wells. SPE J 2016;21(3): 1000−8.

[19] Xu G, Wong S-W. Interaction of multiple non-planar hydraulic fractures in horizontal wells. In: International petroleum Technology Conference; 2013. p. IPTC-17043-MS.

[20] Kumar D, Ghassemi A. Three-dimensional poroelastic modeling of multiple hydraulic fracture propagation from horizontal wells. Int J Rock Mech Min Sci 2018;105:192−209.

[21] Li S, Firoozabadi A, Zhang D. Hydromechanical modeling of nonplanar three-dimensional fracture propagation using an iteratively coupled approach. J Geophys Res Solid Earth 2020;125(8):e2020JB020115.

[22] Bai M, Green S, Suarez-Rivera R. Effect of leakoff variation on fracturing efficiency for tight shale gas reservoirs. In: Alaska rocks 2005, the 40th US symposium on rock Mechanics (USRMS); 2005. p. ARMA-05-697.

[23] Ferrill DA, McGinnis RN, Morris AP, Smart KJ, Sickmann ZT, Bentz M, et al. Control of mechanical stratigraphy on bed-restricted jointing and normal faulting: Eagle Ford Formation, south-central Texas. AAPG (Am Assoc Pet Geol) Bull 2014;98(11):2477−506.

[24] Miskimins JL, Barree RD. Modeling of hydraulic fracture height containment in laminated sand and shale sequences. In: Proceedings of the SPE production and operations symposium. Oklahoma City: OnePetro; 2003.

[25] Rho S, Suarez-Rivera R, Noynaert S. Consequences of rock layers and interfaces on hydraulic fracturing and well production of unconventional reservoirs. Geophysics 2018;83(6). MR333−M344.

[26] Yue K, Olson JE, Schultz RA. The effect of layered modulus on hydraulic-fracture modeling and fracture-height containment. SPE Drill Complet 2019;34(4):356−71.

[27] Dontsov EV. A homogenization approach for modeling a propagating hydraulic fracture in a layered material. Geophysics 2017;82(6). MR153−M162.

[28] Chen B, Barboza BR, Sun Y, Bai J, Thomas HR, Dutko M, et al. A review of hydraulic fracturing simulation. Archives of Computational Methods in Engineering; 2021.

[29] Zhao K, Stead D, Kang H, Damjanac B, Donati D, Gao F. Investigating the interaction of hydraulic fracture with pre-existing joints based on lattice spring modeling. Comput Geotech 2020;122:103534.

[30] Zhao K, Stead D, Kang H, Gao F, Donati D. Three-dimensional numerical investigation of the interaction between multiple hydraulic fractures in horizontal wells. Eng Fract Mech 2021;246:107620.

[31] Elfen TGR Mannual. UK: Rockfield Software LTD; 2020.

[32] Profit M, Dutko M, Yu J, Cole S, Angus D, Baird A. Complementary hydromechanical coupled finite/discrete element and microseismic modelling to predict hydraulic fracture propagation in tight shale reservoirs. Computational Particle Mechanics 2016;3(2):229−48.

[33] Richards GJ, Bere AT, Roberts DT, Thomas SD, Mutlu O, Gaillot PJ. Hydraulic fracturing in heterogenous reservoirs; modelling at petrophysical vs. Geomechanical resolution. In: 54th US rock Mechanics/Geomechanics symposium; 2020. p. ARMA-2020-1842.

[34] Ju Y, Chen J, Wang Y, Gao F, Xie H. Numerical analysis of hydrofracturing behaviors and mechanisms of heterogeneous reservoir glutenite, using the continuum-based discrete element method while considering hydromechanical coupling and leak-off effects. J Geophys Res Solid Earth 2018;123(5):3621−44.

[35] Lobao MC. Finite element modelling of hydraulic fracture flow in porous media. United Kingdom): Swansea University; 2007.

[36] Snow DT. A parallel plate model of fractured permeable media. Berkeley: University of California; 1965.

[37] Bai M. Improved understanding of fracturing tight-shale gas formations. In: SPE production and operations symposium. Oklahoma City, Oklahoma, USA: Society of Petroleum Engineers; 2011. SPE-140968-MS.

[38] Howard GC, Fast C. Optimum fluid characteristics for fracture extension. Conference Optimum fluid characteristics for fracture extension. OnePetro.

[39] Williams BB. Fluid loss from hydraulically induced fractures. J Petrol Technol 1970;22(7):882−8.

[40] Chen M, Zhang S, Xu Y, Ma X, Zou Y. A numerical method for simulating planar 3D multi-fracture propagation in multi-stage fracturing of horizontal wells. Petrol Explor Dev 2020;47(1):171−83.

[41] Wang Y, Ju Y, Zhang H, Gong S, Song J, Li Y, et al. Adaptive finite element−discrete element analysis for the stress shadow effects and fracture interaction behaviours in three-dimensional multistage hydrofracturing considering varying perforation cluster spaces and fracturing scenarios of horizontal wells. Rock Mech Rock Eng 2021;54(4):1815−39.

[42] Crump JB, Conway MW. Effects of perforation-entry friction on bottomhole treating analysis. J Petrol Technol 1988;40(8):1041−8.

[43] Savitski AA, Detournay E. Propagation of a penny-shaped fluid-driven fracture in an impermeable rock: asymptotic solutions. Int J Solid Struct 2002;39(26):6311−37.

[44] Gu H, Siebrits E. Effect of formation modulus contrast on hydraulic fracture height containment. SPE Prod Oper 2008;23(2):170−6.

[45] Huang J, Fu P, Settgast RR, Morris JP, Ryerson FJ. Evaluating a simple fracturing criterion for a hydraulic fracture crossing stress and stiffness contrasts. Rock Mech Rock Eng 2019;52(6):1657−70.

[46] Sesetty V, Ghassemi A. A numerical study of sequential and simultaneous hydraulic fracturing in single and multi-lateral horizontal wells. J Petrol Sci Eng 2015;132:65−76.

[47] Wu K, Olson J, Balhoff MT, Yu W. Numerical analysis for promoting uniform development of simultaneous multiple-fracture propagation in horizontal wells. SPE Prod Oper 2016;32(1):41−50.